1-2006

Cool White Dwarfs in the Sloan Digital Sky Survey

Mukremin Kilic
University of Texas at Austin, kilic@ou.edu

Jeffrey A. Munn
US Naval Observatory, jam@nofs.navy.mil

Hugh C. Harris
US Naval Observatory

James W. Liebert
University of Arizona, Steward Observatory, jamesliebert@gmail.com

Ted von Hippel
Embry-Riddle Aeronautical University, vonhippt@erau.edu

See next page for additional authors

The Astronomical Journal, 131:582–599, 2006 January

COOL WHITE DWARFS IN THE SLOAN DIGITAL SKY SURVEY[1,2]

Mukremin Kilic,[3] Jeffrey A. Munn,[4] Hugh C. Harris,[4] James Liebert,[5] Ted von Hippel,[3]
Kurtis A. Williams,[5] Travis S. Metcalfe,[6] D. E. Winget,[3] and Stephen E. Levine[4]
Received 2004 November 18; accepted 2005 March 28

ABSTRACT

A reduced proper motion diagram utilizing Sloan Digital Sky Survey (SDSS) photometry and astrometry and USNO-B plate astrometry is used to separate cool white dwarf candidates from metal-weak, high-velocity, main-sequence Population II stars (subdwarfs) in the SDSS Data Release 2 imaging area. Follow-up spectroscopy using the Hobby-Eberly Telescope, the MMT, and the McDonald 2.7 m telescope is used to demonstrate that the white dwarf and subdwarf loci separate cleanly in the reduced proper motion diagram and that the contamination by subdwarfs is small near the cool white dwarf locus. This enables large, statistically complete samples of white dwarfs, particularly the poorly understood cool white dwarfs, to be created from the SDSS imaging survey, with important implications for white dwarf luminosity function studies. SDSS photometry for our sample of cool white dwarfs is compared to current white dwarf models.

Key words: stars: atmospheres — stars: evolution — white dwarfs

Online material: color figures, machine-readable table

1. INTRODUCTION

The white dwarf luminosity function of the Galactic disk has traditionally been used as one tool to estimate the star formation history and age of this population (Liebert 1979; Winget et al. 1987; Liebert et al. 1988). The largest samples to date used to determine the white dwarf luminosity function are those of Fleming et al. (1986; see Liebert et al. [2005] for an updated version) on the hot end and Oswalt et al. (1996; using white dwarfs in common proper-motion binaries) on the cool end. The most commonly used luminosity function for cool white dwarfs (Liebert et al. 1988) was based on a sample of only 43 stars selected on the basis of large proper motion from the Luyten half-second proper-motion survey (Luyten 1979a). Questions about completeness and kinematic selection bias have been raised over the years, and the need to construct a larger, deeper, and more complete sample has been obvious. Of even greater interest is the possibility of delineating a useful sample of white dwarfs from the local halo, which may be drawn largely from a single burst of star formation at a greater age than the disk. Oppenheimer et al. (2001) claimed to have found a significant population of halo white dwarfs from kinematic surveys, although these claims were later disputed by several investigators (Reid et al. 2001; Reylé et al. 2001; Silvestri et al. 2002; Bergeron 2003; Spagna et al. 2004).

The Sloan Digital Sky Survey (SDSS; York et al. 2000) offers a valuable new resource that can be used to identify a significantly larger white dwarf sample. Imaging is performed in five broad optical bands (u, g, r, i, and z) down to $\sim$22 mag in u, g, and r with 95% completeness for point sources. Hot white dwarfs can be identified efficiently due to their blue colors (Fan 1999; Kleinman et al. 2004), but white dwarfs near or below the temperatures of Population II main-sequence turnoff stars are buried in the stellar locus. Methods such as the use of an intermediate-band filter to find stars with no MgH absorption feature (Claver 1995) turned out to be less efficient than expected (Kilic et al. 2004). However, the reduced proper motion technique (Luyten 1918) offers an efficient means to identify cooler white dwarfs, as well as halo white dwarfs, by their underluminosity in comparison to main-sequence stars with similar colors and their high space motions.

An improved proper-motion catalog combining the USNO-B (Monet et al. 2003; five epochs) and SDSS catalogs in the area of sky covered by SDSS Data Release 1 (DR1; Abazajian et al. 2003) is presented by Munn et al. (2004). They used SDSS astrometry to recalibrate the USNO-B plate astrometry, reducing both the statistical and systematic errors significantly. In addition, SDSS positions were used to eliminate the large number of false high proper motion objects in the USNO-B catalog.

The combination of accurate SDSS photometry and SDSS + USNO-B astrometry enables us to construct a reduced proper motion diagram and select cool white dwarf candidates from the disk and halo. This paper presents results from the first year of our spectroscopic campaign. In § 2 we present the reduced proper motion diagram from SDSS Data Release 2 (DR2) and review our target selection criteria for follow-up spectroscopy. Our spectroscopic observations are described in § 3, while an analysis of the observational material and results from this analysis are presented in § 4. Various implications of these results are then discussed in § 5.

2. TARGET SELECTION

The reduced proper motion, defined as $H = m + 5 \log \mu + 5$, where m is the apparent magnitude and μ is the proper motion in arcseconds per year, has long been used as a proxy for the absolute magnitude of a star, in a sample with similar kinematics.

[1] Based on observations obtained with the Hobby-Eberly Telescope, which is a joint project of the University of Texas at Austin, Pennsylvania State University, Stanford University, Ludwig-Maximilians-Universität München, and Georg-August-Universität Göttingen.

[2] Observations reported here were obtained at the MMT Observatory, a joint facility of the Smithsonian Institution and the University of Arizona.

[3] Department of Astronomy, University of Texas at Austin, 1 University Station C1400, Austin, TX 78712; kilic@astro.as.utexas.edu.

[4] US Naval Observatory, 10391 West Naval Observatory Road, Flagstaff, AZ 86001-8521.

[5] Steward Observatory, University of Arizona, 933 North Cherry Avenue, Tucson, AZ 85721.

[6] Harvard-Smithsonian Center for Astrophysics, Mail Stop 16, 60 Garden Street, Cambridge, MA 02138.

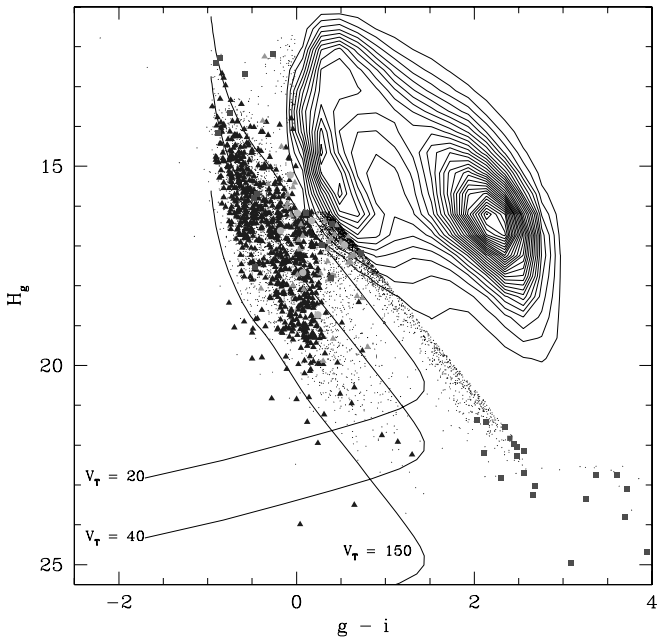

FIG. 1.—Reduced proper motion diagram for stars in the SDSS DR2. Individual stars are plotted only in the region of interest for white dwarfs; the remaining stars are represented by the contours. Previously known white dwarfs, white dwarf + late-type star binaries, subdwarfs, and quasars are shown as dark triangles, light triangles, squares, and circles, respectively. White dwarf cooling curves for different tangential velocities are shown as solid lines. The $V_T = 20$—40 km s^{-1} curves mark the expected location of disk white dwarfs, whereas the $V_T = 150$ km s^{-1} curve represents the halo white dwarfs. [*See the electronic edition of the Journal for a color version of this figure.*]

Munn et al. (2004) presented a reduced proper motion diagram for a portion of SDSS DR1 in their Figure 12. Their SDSS + USNO-B catalog is 90% complete to $g = 19.7$, with proper-motion errors of $\sim$3.5 mas yr^{-1} in right ascension and declination. Four populations are delineated as roughly parallel diagonal distributions in their diagram. The old Population I main sequence is seen in the top right, and the Population II main sequence separates fairly cleanly to the left and extends down past $H_g = 21$ near $g - i = 2$. The white dwarf sequence appears to separate to the left of the Population II subdwarfs, and an unconfirmed extension of this appears as a sequence of objects to higher H_g and redder color.

Figure 1 presents the reduced proper motion diagram for all stars in SDSS DR2 (Abazajian et al. 2004) with $15 < g < 20$ and with reliably measured proper motions greater than 20 mas yr^{-1}. Individual stars are plotted only if they are bluer than $g - i = 0$ or if $H_g > 15.136 + 2.727(g - i)$, a cut that should include all white dwarfs; the remaining vast majority of stars are represented by the contours, as there are too many stars to plot individually. Spectroscopically confirmed white dwarfs, white dwarf plus M dwarf binaries, subdwarfs, and QSOs are plotted as dark triangles, light triangles, squares, and circles, respectively. The spectroscopic identifications are drawn from the SDSS DR1 white dwarf catalog (Kleinman et al. 2004) and QSO catalog (Schneider et al. 2003), and the G. P. McCook & E. M. Sion catalog.[7] We also classified all currently available SDSS spectra for stars in the diagram with $g - i > 0$ or $H_g > 19$ and that had not previously been classified (190 objects total). The expected sequences of white dwarfs (pure H atmosphere, $\log g = 8$) for specific tangential velocities (V_T) are shown as solid lines, where colors and absolute magnitudes are predicted using model atmospheres from P. Bergeron (2001, private communication). The $V_T = 20$–40 km s^{-1} curves mark the expected location of disk white dwarfs, whereas the $V_T = 150$ km s^{-1} curve represents the halo white dwarfs. The white dwarf cooling curves pass through the locus of hotter white dwarfs, then make a sharp turn due to the onset of collision-induced absorption (CIA) due to molecular hydrogen for the coolest stars with pure H atmospheres (Hansen 1998; Saumon & Jacobson 1999); this opacity depresses the i band, making the colors turn bluer.

Defining a "reliable" proper motion is important, as even a small fraction of stars with falsely measured large proper motions will scatter from the very densely populated subdwarf turnoff region of the reduced proper motion diagram into the sparsely populated region expected to contain the cool white dwarfs. We adopt a prescription for a reliably measured proper motion similar to that delineated by Munn et al. (2004) for their catalog: (1) the SDSS detection in both the g and i band must match the "clean" criteria as described in the DR1 documentation, (2) there must be a one-to-one match between the SDSS and USNO-B objects, and (3) the proper-motion fit must have an rms residual of less than 525 mas in each coordinate. We further require the star to have been detected in all five epochs in USNO-B and the distance to the nearest neighbor with $g < 22$ to exceed 7″. The final two requirements are based on inspection of all the plate images used in the USNO-B catalog for a subsample of 562 stars in the portion of the reduced proper motion diagram expected to be populated by halo and cool disk white dwarfs ($-1 < g < 1.5$ and $H_g > 18$) with proper motions greater than 100 mas yr^{-1} (the reality of measured proper motions smaller than that was too difficult to judge using the quick by-eye inspections we employed). Of the 201 inspected stars that were detected in all five USNO-B epochs and whose nearest neighbors (brighter than $g = 22$) are greater than 7″ away, only three were judged to have a falsely measured large proper motion, for a 1.5% contamination rate. On the other hand, of the 20 inspected stars that were detected in all five USNO-B epochs but had neighbors closer than 7″, seven were judged to have an incorrectly measured proper motion, for a contamination rate of 35%. Objects separated by less than 7″ tend to be blended on the Schmidt plates, leading to incorrectly measured proper motions. All 208 inspected stars that were not detected in one or two of the USNO-B epochs and that have a nearest neighbor closer than 7″ had incorrectly measured proper motions. The contamination rate of falsely measured large proper motions increases for stars not detected in all five USNO-B epochs, even if their nearest neighbors are greater than 7″ away. For such stars, 20 of 39 inspected stars not detected in one of the USNO-B epochs had incorrectly measured proper motions, for a contamination rate of 51%, while 81 of 91 not detected in two of the USNO-B epochs had incorrectly measured proper motions, for a contamination rate of 89%.

In Figure 1 it is clear that the hot white dwarfs previously targeted spectroscopically by SDSS are well separated from the main-sequence and subdwarf stars (represented by the contours) and are located where expected from the models. It is also clear that the white dwarf locus extends more to the red and to larger reduced proper motion, well separated from the subdwarf locus (the diagonal cut where we start to plot individual stars), and that SDSS has not spectroscopically observed these cooler white dwarf candidates. This drove our target selection. Our goal was to obtain spectroscopic identifications for a large sample of cool white dwarf candidates so as to understand the efficiency of using reduced proper motions to select cool white dwarfs, as well as the contamination due to subdwarfs. Thus, we

[7] VizieR Online Data Catalog, III/235 (G. P. McCook & E. M. Sion, 2003).

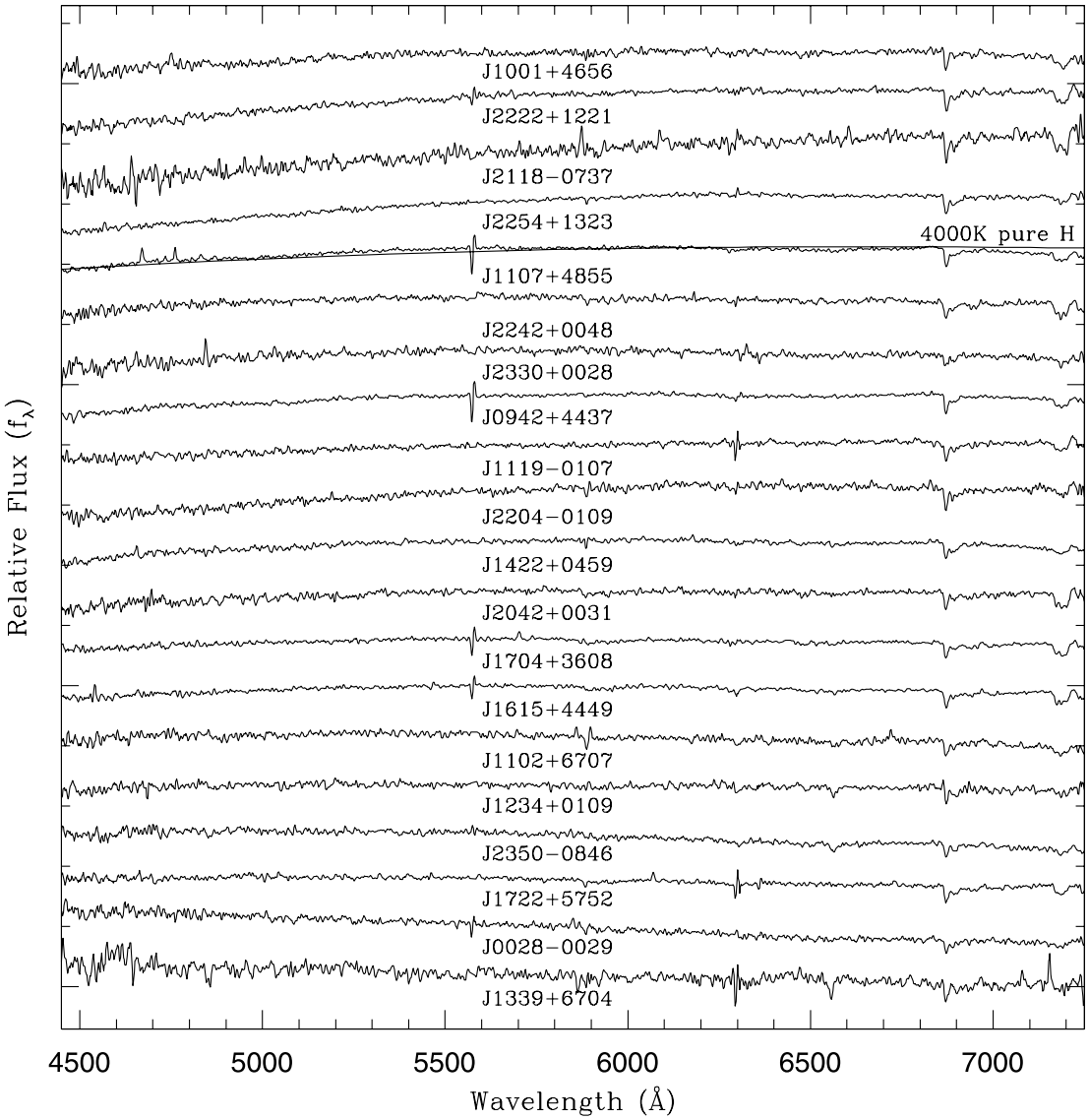

FIG. 2.—Optical spectra for white dwarfs observed at the HET. The spectra are normalized at 5500 Å and are shifted vertically from each other by arbitrary units. The synthetic spectrum of a 4000 K pure H atmosphere white dwarf (D. Saumon 2002, private communication) is also shown. The $g - r$ color increases from bottom to top.

selected most of our targets from the region with $g - i > 0$ and to the left of the $V_T = 20$ km s^{-1} curve, although we also selected some to the right of the curve to better understand how cleanly the white dwarf and subdwarf loci separate.

3. OBSERVATIONS

Follow-up spectroscopy of the cool white dwarf candidates was obtained at the Hobby-Eberly Telescope (HET), the MMT, and the McDonald 2.7 m Harlan Smith Telescope between 2003 September and 2004 October (an additional observing run with the Kitt Peak 4 m telescope was completely lost to weather). We used the HET equipped with the Marcario Low Resolution Spectrograph (LRS) to obtain low-resolution spectroscopy of 22 cool white dwarf candidates. Grism 2 with a 1.″5 slit produced spectra with a resolution of 6 Å over the range 4280–7340 Å. Spectroscopy for 56 additional stars was obtained at the MMT with the Blue Channel Spectrograph and the 500 lines mm^{-1} grating, which produced spectra with a resolution of 3.6 Å over the range 3640–6800 Å. In addition, we obtained spectroscopy for 89 stars at the McDonald 2.7 m telescope with the Large Cassegrain Spectrograph and TI1 camera using grating 43 (600 lines mm^{-1}), which produced spectra with a resolution of 5.2 Å over the range 3870–5260 Å. In each case, a spectrophotometric standard star was observed each night for flux calibration. Ne-Cd, He-Ar-Ne, and Ar calibration lamp exposures were taken after each observation with the HET, the MMT, and the McDonald 2.7 m telescope, respectively. The data were reduced using standard IRAF[8] routines.

The spectra for all the observed white dwarfs at the HET, the MMT, and the McDonald 2.7 m telescope are shown in Figures 2, 3, and 4, respectively. The spectra are ordered in decreasing $g - r$ color for Figures 2 and 3 and decreasing $u - r$ color for Figure 4. The majority of the objects observed at the HET and the MMT are featureless cool DC white dwarfs. The only features seen in these spectra are due to sky-subtraction problems at λ5577, $\lambda\lambda$5890, 5896, λ6300, and the atmospheric B band at 6890 Å. Several

[8] IRAF is distributed by the National Optical Astronomy Observatory, which is operated by the Association of Universities for Research in Astronomy, Inc., under cooperative agreement with the National Science Foundation.

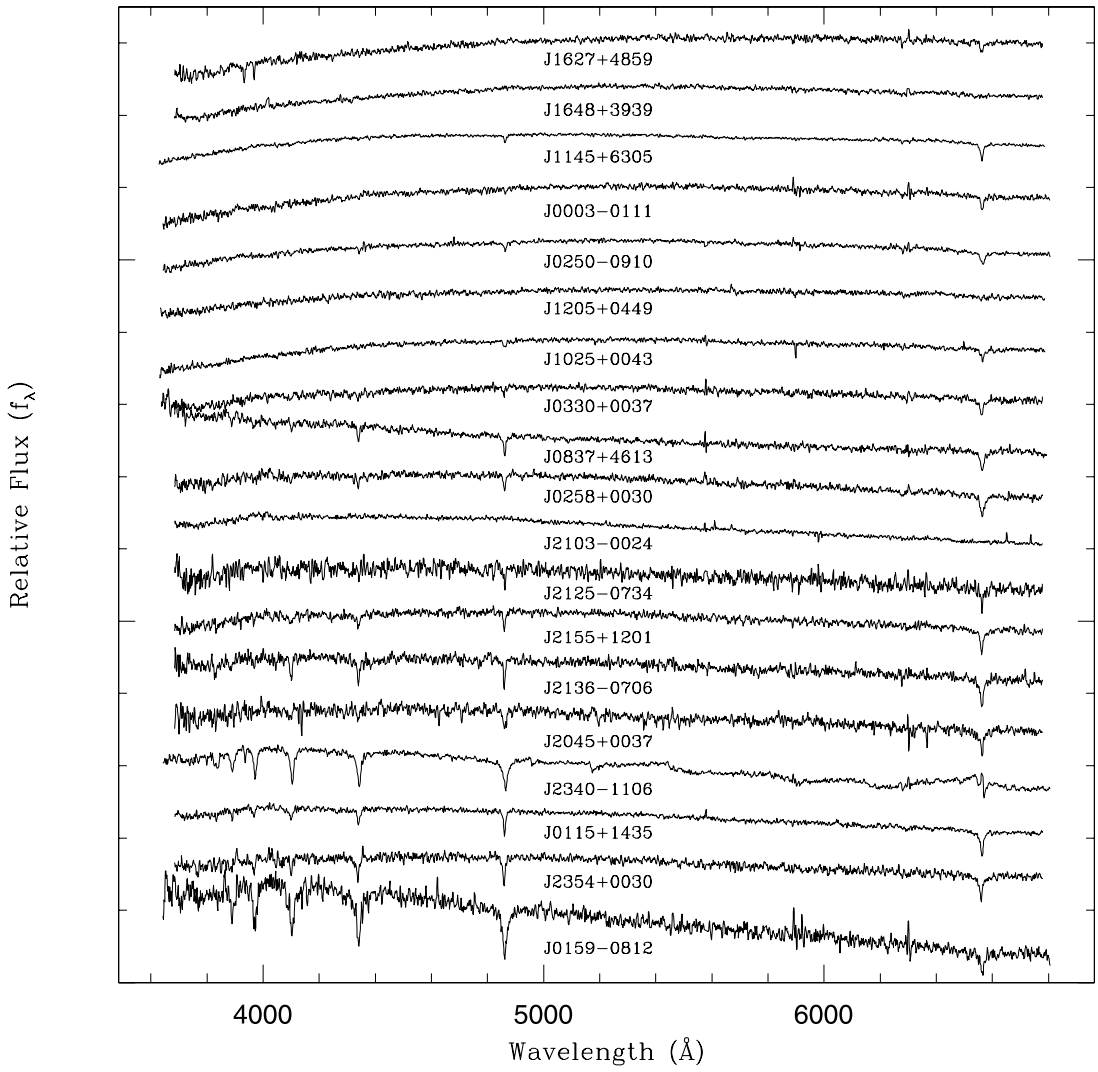

FIG. 3.—Same as Fig. 2, but for white dwarfs observed at the MMT.

white dwarfs show only a weak Hα line and are DA white dwarfs with probable cool, hydrogen-rich atmospheres. Most of the brighter objects observed at the McDonald 2.7 m telescope are DA white dwarfs. Three objects clearly show additional features due to late-type star companions (J0929+5547, J1336+0017, and J2340−1106). Two objects observed at the 2.7 m telescope are magnetic DAs (J1011+0029 and J1144+6629), while two other objects observed at the 2.7 m telescope and an additional three objects observed at the MMT are DZAs with detectable Ca II H and K lines and Balmer lines (J0045+1420, J0748+3506, J1627+4859, J1654+3829, and J2154+1300). We also note that four previously known white dwarfs, namely, SDSS J0109−1042 (LP 707-8), J0755+3621 (WD 0752+365), J1025+0043 (LHS 282), and J1145+6305 (WD 1143+633), were observed at the MMT and the McDonald 2.7 m telescope and are included in Figures 3 and 4.

The biggest difficulty in classifying the spectra is to distinguish DZ, DZA, and DAZ white dwarfs[9] with refractory heavy elements from nondegenerate probable main-sequence stars (subdwarf F, G, and K types) with low, scaled-solar heavy elements. Ca appears most frequently in DZ, DAZ, and DZA stars, followed by Mg, Fe, and occasionally Na. The white dwarfs apparently never show the CH band (4300 Å), which is detected for sdG and cooler stars ($g - i > 0.4$), and do not show MgH and CaH, which appear in progressively cooler sdK stars.

Figure 5 shows the spectra for several subdwarfs observed at the MMT. The spectra are plotted in order of decreasing $T_{\rm eff}$, represented by increasing $g - i$ color. This figure demonstrates that subdwarfs have Ca II (and hence need MMT and McDonald 2.7 m telescope blue coverage) and usually many other metal features plus the CH molecular band. Additional MgH and CaH bands can be seen among cooler subdwarfs (without enough blue coverage, HET was mostly used to observe cool white dwarf candidates with colors similar to those of G and K type subdwarfs). We paid close attention to the $u - g$ and $g - r$ colors of each star, comparing colors of each candidate with white dwarf model colors to see if they were consistent with the strengths of the hydrogen lines, and to the degree to which cool DA Balmer decrements steepened until only Hα was seen in the coolest DAs.

Our classifications and additional data for the 112 spectroscopically confirmed white dwarfs and 55 subdwarfs from this study are given in Tables 1 and 2, respectively. Positions are those from the SDSS astrometric pipeline (Pier et al. 2003). The

[9] Note that the difference between DAZ and DZA stars is whether the dominant atmospheric constituent is hydrogen or helium, respectively. DZA stars show steep Balmer decrements at higher $T_{\rm eff}$ than DAZ stars.

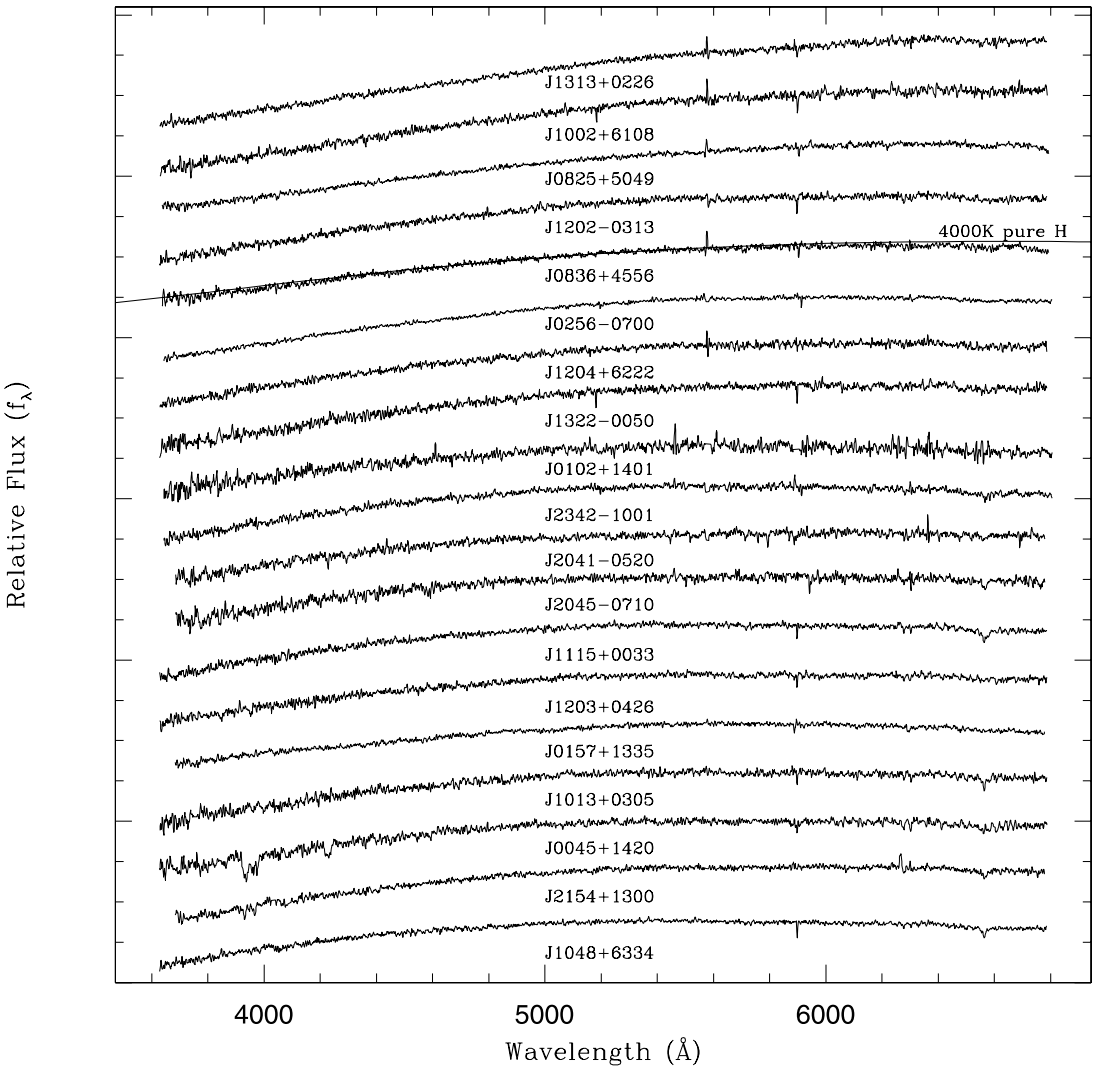

FIG. 3.—*Continued*

photometric calibration is based on the SDSS standard star system (Smith et al. 2002) tied to the survey data with the Photometric Telescope (Hogg et al. 2001). Interstellar absorption A_u from Schlegel et al. (1998) and fully dereddened magnitudes and colors are given for each object. Tables 1 and 2 also give the proper motions in each component and the number of epochs in which an object is detected. In addition, the effective temperatures, photometric distances, and tangential velocities for the newly discovered cool white dwarfs (see § 4.4) are also given in Table 1.

A few stars in Table 1 were previously known as likely white dwarfs. The most certain case is SDSS J131313.12+022645.8 (LHS 2696), which has a (preliminary) parallax in Dahn et al. (1989). There are 13 additional stars discovered in the New Luyten Two Tenths Catalog (Luyten 1979b, hereafter NLTT), most with Luyten color class a, f, or g, that would have been considered to be nearly certain white dwarfs on the basis of the NLTT data alone; the spectra in this paper now confirm these classifications. The one very cool white dwarf in Table 1 that is also in the NLTT catalog is SDSS J075313.28+423001.6 (LP 207-50). It has color class m in the NLTT, so would not be considered as a white dwarf from the NLTT data alone. In addition, three stars in Table 1 were identified from their proper motion by Lépine et al. (2003): SDSS J100225.85+610858.1 (LSR 1002+ 6108), SDSS J110731.38+485523.0 (LSR 1107+4855), and SDSS J222233.90+122143.0 (LSR 2222+1221). The first two were classified as probable white dwarfs and the third as a probable subdwarf on the basis of their reduced proper motion and photographic colors.

4. RESULTS

4.1. *Reduced Proper Motion Diagram*

Figure 6 repeats the reduced proper motion diagram of Figure 1, except that the spectroscopic identifications presented in this paper are indicated rather than previously known identifications. Again, this is limited to stars with reliable proper motions, that is, stars detected in all five USNO-B epochs and with no neighbor brighter than $g = 22$ within $7''$. There is a clean separation between the white dwarfs and subdwarfs. Of the 95 spectroscopically confirmed stars bluer than $g - i = 1.5$ and below the $V_T = 20$ km s^{-1} curve, corresponding to the region in which we expect to find only white dwarfs, 91 are certain white dwarfs, two are certain subdwarfs, and two are probable white dwarfs for which a classification of subdwarf cannot be ruled out. Visual inspection of the plate images reveals that the two subdwarfs had falsely measured large proper motions, consistent with the contamination rate derived earlier for our adopted reliable

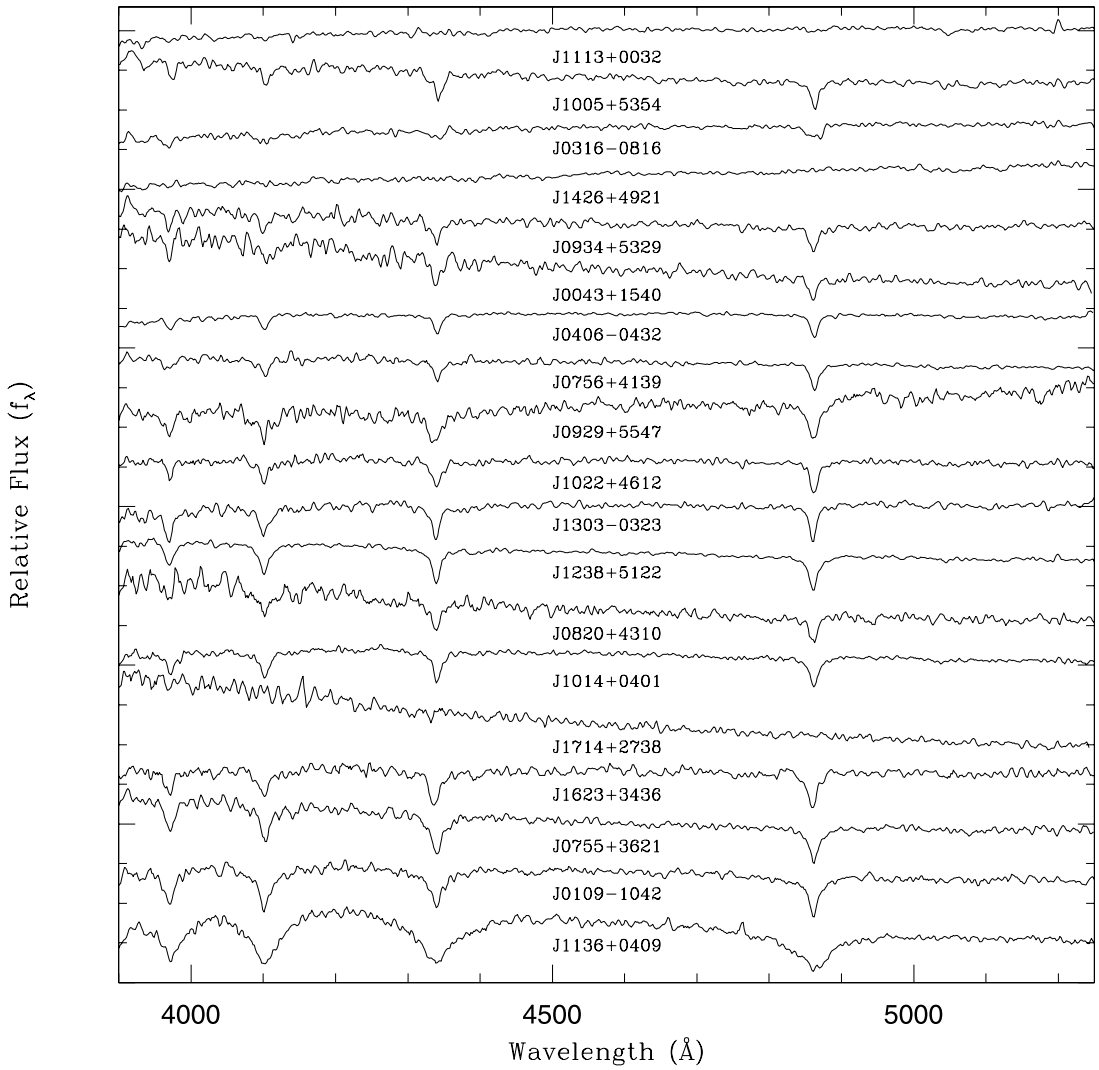

FIG. 4.—Optical spectra for white dwarfs observed at the McDonald 2.7 m Harlan Smith Telescope. The spectra are normalized at 4600 Å and are shifted vertically from each other by arbitrary units. The $u - r$ color increases from bottom to top.

proper-motion criteria, while the two probable white dwarfs had correctly measured proper motions.

Figure 7 shows the MMT spectra for these two probable white dwarfs. SDSS J2236+1419 ($H_g = 18.75$ and $g - i = 0.52$) shows Mg I λ3830, Ca II $\lambda\lambda$3933, 3968, Ca I λ4226, Na I λ5892, and probable Mg I λ5175, with no detectable Hα, Hβ, and CH band. The absent H and CH features suggest a very non–Population II, (scaled solar) metallicity, DZ white dwarf. SDSS J1214+6216 ($H_g = 21.97$ and $g - i = 0.64$) shows Mg I λ3830, Ca II, no Ca I, no CH, weak Hβ, possible Na I λ5892, and rather strong Hα. The steep H decrement is consistent with a cool white dwarf with pressure broadening, quenching the higher Balmer levels. Again, the absent CH is probably inconsistent with an sdG. We classify this object as a probable DZA white dwarf, pending detailed analysis. Assuming that these two objects are white dwarfs, we find no contamination from subdwarfs with correctly measured proper motions. On the other hand, if we assume that these objects are in fact subdwarfs, they would represent subdwarfs that truly have scattered into the cool white dwarf region of the reduced proper motion diagram; there is still potential for some genuine contamination from subdwarfs.

We also observed stars that did not meet our criteria for a reliable proper motion, either having not been detected in one or two USNO-B epochs or having a neighbor within 7″. Of these, 16 were white dwarfs (Fig. 6, *asterisks*), all located within the white dwarf region of the reduced proper motion diagram; on visual inspection of the plates used in USNO-B, all the measured proper motions were correct. Another 37 were subdwarfs (see Table 2), located in both the white dwarf and subdwarf regions of the reduced proper motion diagram; visual inspection shows all but three of these to have incorrectly measured proper motions, and the proper motions of the remaining three were too small to determine their validity by eye.

The reduced proper motion diagram, using our conservative criteria for a reliable proper motion, can thus be used to define a statistically complete sample of white dwarfs, including the coolest white dwarfs, which are difficult to efficiently select using other techniques. There is a roughly 1.5% contamination rate of incorrectly measured proper motions. There is likely no contamination due to subdwarfs with correctly measured proper motions, although contamination of a few percent is still possible. True white dwarfs that fail to meet the proper-motion criteria must be accounted for, either statistically or by using visual inspection to verify proper motions for all candidates. This result is used in Harris et al. (2006) to construct the white dwarf luminosity function using the SDSS Data Release 3 imaging and USNO-B astrometry.

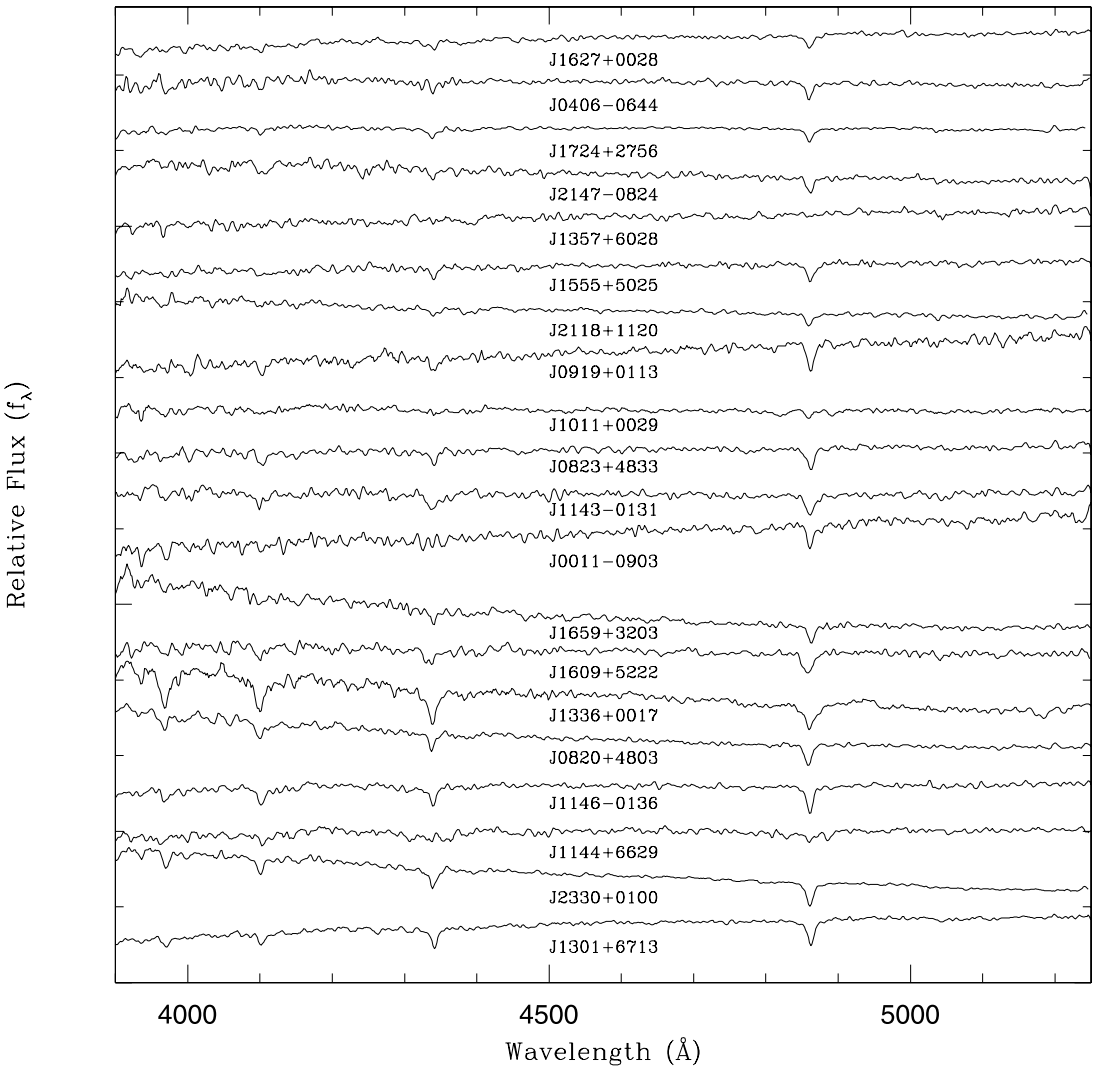

FIG. 4.—*Continued*

4.2. *Color-Color Diagrams*

SDSS color-color diagrams for spectroscopically identified proper-motion objects are shown in Figure 8. The spectral classifications are indicated in the diagrams, and contours that show the colors of nondegenerate stars in the SDSS are included for comparison. The curves show the colors of white dwarf model atmospheres of pure H (*solid curves*) and pure He (*dashed curves*) composition with $\log g = 7$, 8, and 9, kindly made available to us by P. Bergeron.

Harris et al. (2003) showed that the sequence of white dwarfs hotter than 12,000 K is contaminated only by hot subdwarfs. Our $u - g$ versus $g - r$ color-color diagram demonstrates that white dwarfs and subdwarfs selected from the reduced proper motion diagram separate from each other for $u - g \leq 1.0$, although this result depends on a handful of white dwarfs observed over the range $0.6 \leq u - g \leq 1.0$, and further observations are needed to confirm this result.

Figure 8 (*top left*) also shows that the cool white dwarf model atmospheres cannot predict the $u - g$ colors below 6000 K accurately, although the $g - r$, $r - i$, and $i - z$ colors agree reasonably well with the observed sequence of cool white dwarfs (see Fig. 8, *top right, bottom*). Bergeron et al. (1997) were the first to introduce a UV opacity source in the coolest hydrogen-rich white dwarf models in terms of a pseudocontinuum opacity to fit the observed hydrogen-rich cool white dwarf sequence. They found that this opacity source is needed to explain the observed UV colors of cool hydrogen-rich white dwarfs below 5300 K. This is also seen in the $B - V$ versus $V - K$ color-color diagram of Bergeron et al. (2001) and the $r -$ DDO51 versus $r - z$ color-color diagram of Kilic et al. (2004). Wolff et al. (2002) showed that this UV flux deficiency (relative to model atmosphere predictions) extends even more strongly into the space ultraviolet region (2000–3200 Å). Here we find that the $u - g$ colors for neither cool DA nor cool DC white dwarfs can be explained with the current model atmospheres. Significant improvements are needed in the cool white dwarf model atmospheres to understand the unexplained UV opacity that is crucial for the coolest white dwarfs. In fact, this may be the reason why efforts to fit the spectral energy distributions of ultracool white dwarfs fail.

The majority of the cool white dwarfs with $r - i > 0.25$ ($T_{\rm eff} < 5000$ K) tend to have bluer $i - z$ colors compared to the model predictions (see Fig. 8, *bottom*); the observed blue turnoff of cool white dwarfs is at a bluer color than expected from the models. All but four of the cool white dwarfs occupy a region to the left of $\log g = 9$ (*leftmost line*) white dwarf models. This implies that either all of the very cool white dwarfs are massive, they have mixed H/He atmospheres, or our understanding of the CIA

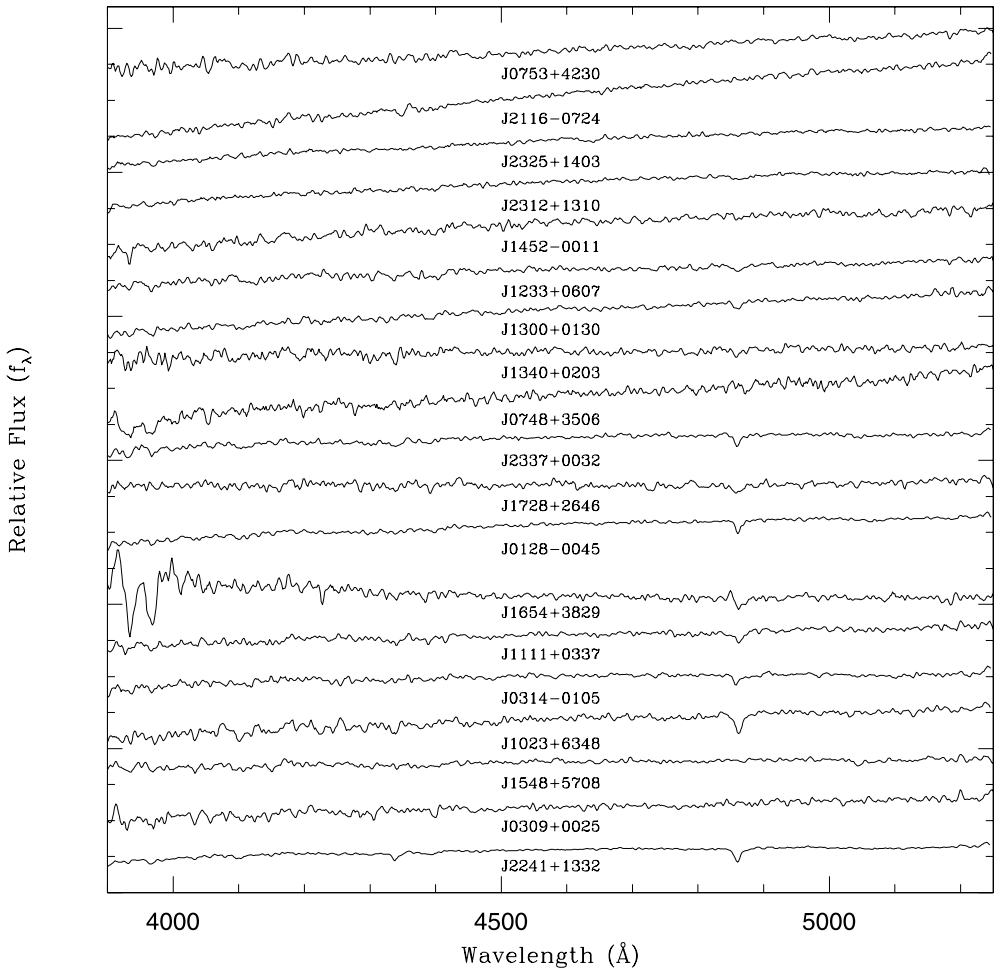

FIG. 4.—*Continued*

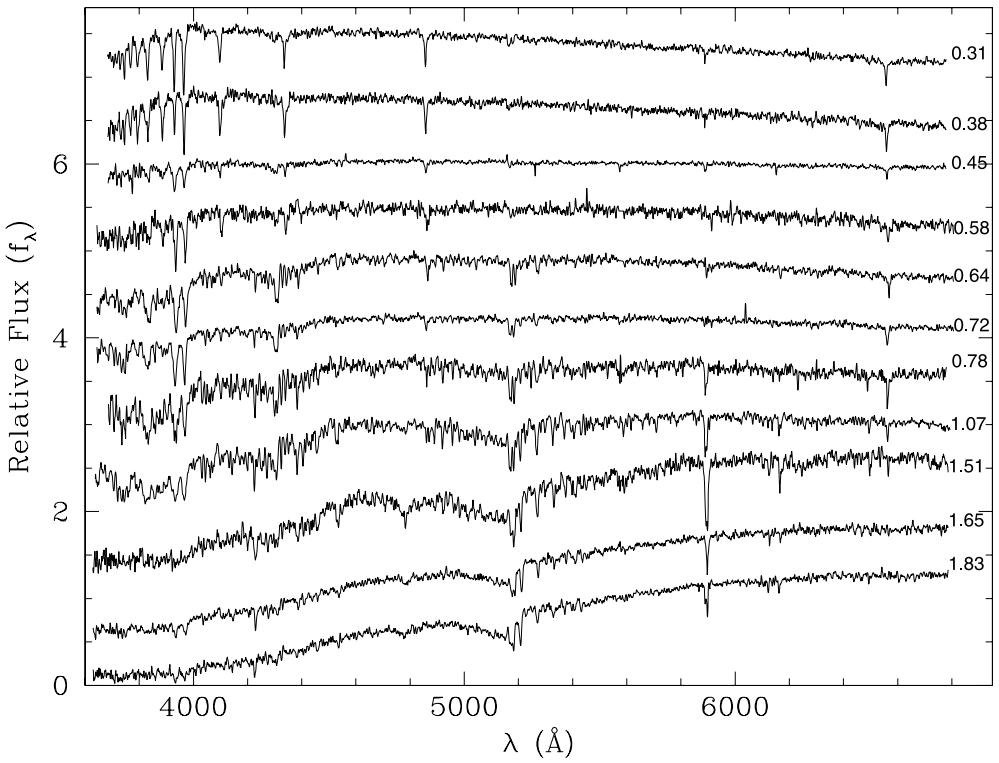

FIG. 5.—Optical spectra of several subdwarf stars observed at the MMT. The spectra are ordered in increasing $g - i$ color, which is given on the right edge of each spectrum.

TABLE 1

SPECTROSCOPICALLY IDENTIFIED WHITE DWARFS

Object (SDSS J) (1)	g (2)	$u-g$ (3)	$g-r$ (4)	$r-i$ (5)	$i-z$ (6)	A_u (7)	$\mu_{\rm R.A.}$ (8)	$\mu_{\rm decl}$ (9)	Epochs (10)	Type (11)	$T_{\rm eff}$ (12)	$M_{\rm bol}$ (13)	M_g (14)	D (15)	V_T (16)	Source (17)
000316.69−011117.9	19.21	1.22	0.49	0.22	0.02	0.16	98	−16	6	DA	5351	14.57	15.14	69.19	32.57	MMT
001142.67−090324.3	17.73	0.64	0.31	0.12	0.01	0.21	4	−134	6	DA	6125	13.97	14.37	50.31	31.97	2.7 m
002837.06−002928.9	19.68	0.54	0.36	0.04	−0.11	0.10	103	67	6	DC	6381	13.80	14.16	128.79	75.01	HET
004316.02+154059.5	18.11	0.53	0.18	0.01	−0.05	0.28	−37	25	6	DA	6844	13.49	13.82	79.16	16.76	2.7 m
004521.88+142045.3	18.81	1.35	0.63	0.21	0.03	0.55	260	−53	6	DZA	4732	15.11	15.90	45.73	57.51	MMT
010259.98+140108.1	19.29	1.71	0.73	0.27	0.11	0.22	12	106	6	DC	4582	15.25	16.10	46.84	23.68	MMT
011514.73+143557.5	18.54	0.52	0.25	0.09	−0.02	0.31	−45	−55	4	DA	6320	13.84	14.21	81.60	27.49	MMT
012827.47−004512.6	17.74	1.02	0.37	0.15	0.00	0.16	147	−43	6	DA	5854	14.18	14.62	44.54	32.33	2.7 m
015743.25+133558.2	19.15	1.19	0.64	0.16	0.05	0.25	87	−62	6	DC	5040	14.84	15.51	57.63	29.18	MMT
015938.43−081242.4	19.80	0.42	0.09	−0.10	0.01	0.13	322	−119	6	DA	8214	12.69	13.01	230.40	374.90	MMT
025005.81−091002.8	18.87	1.06	0.48	0.18	0.05	0.15	106	2	6	DA	5474	14.47	15.00	62.59	31.45	MMT
025641.62−070033.8	18.81	1.73	0.80	0.34	0.08	0.26	373	−202	6	DC	4211	15.62	16.56	30.94	62.22	MMT
025854.42+003040.4	18.84	0.73	0.27	0.06	−0.07	0.42	−80	16	6	DA	6189	13.93	14.32	92.32	35.70	MMT
030924.87+002525.3	17.75	0.84	0.34	0.13	−0.02	0.57	−6	−106	6	DC	5637	14.34	14.83	46.60	23.45	2.7 m
031449.81−010519.3	18.31	0.88	0.38	0.12	−0.04	0.39	−77	−71	6	DA	5709	14.29	14.76	58.48	29.03	2.7 m
031613.90−081637.6	16.63	0.56	0.17	0.02	−0.04	0.48	90	−103	6	DA	6610	13.64	13.99	39.65	25.71	2.7 m
033054.88+003716.5	19.33	0.81	0.34	0.10	0.01	0.57	77	34	6	DA	5690	14.30	14.78	98.78	39.41	MMT
040632.39−043250.4	17.02	0.53	0.17	0.00	−0.10	0.56	171	80	6	DA	6624	13.63	13.98	48.89	43.75	2.7 m
040647.32−064436.9	17.70	0.74	0.34	0.07	0.03	0.45	67	27	6	DA	5884	14.15	14.59	48.70	16.67	2.7 m
074811.90+350632.4	18.08	1.13	0.36	0.09	−0.07	0.30	−44	−141	6	DZA	5925	14.12	14.55	56.16	39.32	2.7 m
075313.28+423001.6	17.91	1.84	0.84	0.30	0.10	0.23	113	−403	6	DC	4226	15.61	16.54	20.36	40.39	2.7 m
075631.11+413950.9	16.76	0.52	0.18	0.03	−0.05	0.20	−9	−349	6	DA	6951	13.42	13.75	42.59	70.48	2.7 m
082036.99+431005.3	17.40	0.49	0.08	0.03	−0.09	0.33	−63	−103	6	DA	7192	13.27	13.59	64.72	37.04	2.7 m
082056.07+480352.9	17.16	0.62	0.24	0.12	−0.06	0.22	224	−80	6	DA	6388	13.79	14.16	42.91	48.37	2.7 m
082307.81+483316.6	17.79	0.74	0.25	0.10	−0.02	0.22	−217	−72	6	DA	6378	13.80	14.16	57.26	62.06	2.7 m
082519.70+504920.1	19.17	1.72	0.86	0.33	0.05	0.24	−331	−330	6	DC	4048	15.79	16.74	33.42	74.04	MMT
083641.56+455658.7	19.89	1.63	0.84	0.27	0.15	0.15	−64	−169	6	DC	4373	15.46	16.36	53.19	45.56	MMT
083712.30+461325.1	18.39	0.69	0.29	0.09	0.00	0.14	−80	−40	6	DA	6363	13.81	14.18	72.90	30.90	MMT
091948.92+011353.0	18.21	0.73	0.30	0.11	0.00	0.13	137	−193	6	DA	6227	13.90	14.29	63.81	71.58	2.7 m
092903.12+554758.5	17.85	0.43	0.23	1.05	0.87	0.15	−350	−18	6	DA + M	6719	13.57	13.91	64.55	107.23	2.7 m
093438.94+532937.4	17.47	0.51	0.20	0.04	−0.01	0.06	−151	−145	6	DA	6976	13.40	13.73	57.12	56.68	2.7 m
094244.96+443743.1	19.44	1.92	0.88	0.37	0.19	0.06	−135	−189	6	DC	4052	15.79	16.73	35.66	39.25	HET
100119.48+465650.6	19.24	2.06	1.06	0.33	0.09	0.07	−17	−339	6	DC	3284	16.71	17.48	23.08	37.13	HET
100225.85+610858.1	19.34	2.32	0.96	0.38	0.18	0.08	−448	−328	6	DC	3581	16.33	17.20	27.79	73.15	MMT
100521.05+535408.4	18.02	0.50	0.24	0.05	−0.02	0.04	−145	−219	6	DA	6800	13.52	13.85	68.91	85.79	2.7 m
101105.63+002944.4	17.23	0.69	0.31	0.11	−0.02	0.18	−219	55	6	DAH	6184	13.93	14.32	40.48	43.33	2.7 m
101359.85+030553.8	18.60	1.37	0.63	0.23	0.10	0.16	107	−101	6	DA	4964	14.90	15.60	42.00	29.29	MMT
101414.45+040137.4	16.76	0.46	0.11	0.01	−0.06	0.11	−199	26	6	DA	7506	13.08	13.40	48.78	46.41	2.7 m
102210.36+461249.2	16.42	0.42	0.20	0.05	−0.06	0.07	9	−121	6	DA	6993	13.39	13.72	35.38	20.35	2.7 m
102356.10+634833.8	18.08	0.86	0.34	0.09	0.00	0.05	−344	−216	6	DA	6243	13.89	14.28	58.47	112.58	2.7 m
104801.84+633448.9	17.90	1.43	0.61	0.29	0.02	0.04	−258	−142	6	DA	5004	14.87	15.55	29.94	41.79	MMT
110213.70+670752.6	19.55	1.74	0.65	0.29	0.03	0.09	−380	−185	6	DC	4840	15.01	15.76	59.24	118.67	HET
110731.38+485523.0	19.39	2.02	0.92	0.30	0.12	0.11	−726	−79	6	DC	4020	15.82	16.77	34.85	120.64	HET
111154.54+033726.2	18.22	0.91	0.37	0.11	0.06	0.21	−371	−127	6	DA	5899	14.14	14.57	57.72	107.28	2.7 m
111306.26+003243.7	17.60	0.53	0.21	−0.07	−0.04	0.34	−363	−89	6	DC	6953	13.42	13.75	65.60	116.21	2.7 m
111536.96+003317.3	17.75	1.52	0.66	0.24	0.05	0.23	37	−250	6	DA	4816	15.04	15.79	26.57	31.83	MMT
111940.62−010755.1	19.79	2.01	0.85	0.24	0.15	0.23	−291	−28	6	DC	4283	15.55	16.47	49.77	68.97	HET

TABLE 1—*Continued*

Object (SDSS J) (1)	g (2)	$u-g$ (3)	$g-r$ (4)	$r-i$ (5)	$i-z$ (6)	A_u (7)	$\mu_{\rm R.A.}$ (8)	$\mu_{\rm decl}$ (9)	Epochs (10)	Type (11)	$T_{\rm eff}$ (12)	$M_{\rm bol}$ (13)	M_g (14)	D (15)	V_T (16)	Source (17)
113655.18+040952.6	16.98	0.45	−0.10	0.32	0.51	0.12	−96	−53	4	DA	10077	11.79	12.18	95.28	49.52	2.7 m
114352.16−013149.4	17.36	0.72	0.24	0.09	−0.02	0.10	−277	−2	6	DA	6594	13.65	14.00	48.57	63.78	2.7 m
114439.54+662928.5	17.47	0.62	0.22	0.04	−0.06	0.05	−145	−20	6	DAH	6919	13.44	13.77	55.76	38.68	2.7 m
114625.77−013636.9	16.48	0.59	0.25	0.12	−0.06	0.07	358	−434	6	DA	6516	13.70	14.05	31.35	83.61	2.7 m
120200.48−031347.4	19.86	2.37	0.85	0.32	0.06	0.15	−73	134	6	DC	4151	15.69	16.62	47.03	34.01	MMT
120328.65+042653.4	18.11	1.36	0.66	0.28	0.08	0.10	−252	156	6	DC	4852	15.00	15.75	30.66	43.07	MMT
120439.54+622216.4	19.16	1.69	0.78	0.29	0.10	0.10	−21	−159	6	DC	4528	15.31	16.17	40.92	31.11	MMT
120529.15+044935.6	18.45	0.89	0.48	0.19	0.07	0.09	−138	−53	6	DC	5524	14.43	14.94	51.65	36.19	MMT
123322.45+060710.7	18.21	1.32	0.55	0.19	0.03	0.09	−79	−352	6	DA	5302	14.61	15.19	41.41	70.80	2.7 m
123408.12+010947.4	19.73	1.40	0.54	0.25	0.03	0.13	−284	−55	6	DA	5177	14.72	15.34	79.01	108.34	HET
123847.85+512207.4	17.32	0.46	0.12	−0.02	−0.13	0.07	−319	−21	6	DA	7710	12.96	13.29	65.38	99.06	2.7 m
130021.25+013045.5	17.74	1.23	0.54	0.18	0.12	0.10	−374	145	6	DA	5297	14.61	15.20	33.48	63.66	2.7 m
130121.14+671307.4	16.69	0.56	0.25	0.09	−0.04	0.06	151	52	4	DA	6629	13.63	13.97	35.51	26.88	2.7 m
130313.03−032323.9	16.81	0.45	0.16	0.02	−0.09	0.13	32	−137	6	DA	7160	13.29	13.62	45.47	30.32	2.7 m
131313.12+022645.8	18.84	2.04	1.07	0.37	0.18	0.14	−744	−116	6	DC	3394	16.56	17.38	20.23	72.21	MMT
132254.60−005042.8	18.82	1.75	0.76	0.31	0.09	0.14	−156	118	6	DC	4505	15.33	16.20	35.08	32.52	MMT
133616.05+001732.7	17.34	0.51	0.36	0.76	0.58	0.12	−278	−141	6	DA + M	6116	13.98	14.38	40.76	60.23	2.7 m
133939.55+670449.8	19.79	0.75	0.28	0.12	−0.02	0.07	−194	235	5	DA	6409	13.78	14.14	137.61	198.77	HET
134043.35+020348.3	18.01	1.11	0.43	0.20	0.04	0.13	−534	28	6	DC	5600	14.37	14.87	44.45	112.66	2.7 m
135758.43+602855.3	18.04	0.72	0.35	0.11	−0.05	0.07	−304	55	6	DC	6186	13.93	14.32	56.53	82.78	2.7 m
142225.73+045939.7	19.34	1.54	0.83	0.30	0.08	0.15	−277	−62	6	DC	4365	15.47	16.37	41.08	55.27	HET
142659.40+492100.6	16.93	0.55	0.18	0.07	−0.09	0.11	−96	44	6	DC	6927	13.43	13.77	44.52	22.28	2.7 m
145224.95−001134.7	18.25	1.36	0.58	0.20	0.07	0.27	155	129	6	DC	5052	14.83	15.49	38.98	37.26	2.7 m
154835.89+570826.4	17.70	0.80	0.39	0.13	0.05	0.06	−220	−138	6	DC	5975	14.08	14.50	44.38	54.64	2.7 m
155534.18+502547.8	16.70	0.75	0.31	0.13	0.00	0.10	−234	−5	6	DA	6204	13.92	14.31	31.13	34.54	2.7 m
160920.13+522239.6	18.21	0.65	0.25	0.12	0.01	0.10	155	281	6	DA	6467	13.73	14.09	68.91	104.82	2.7 m
161544.67+444942.5	19.56	1.63	0.75	0.27	0.08	0.05	44	−237	6	DC	4698	15.14	15.95	53.41	61.02	HET
162324.05+343647.7	17.18	0.39	0.11	0.08	0.45	0.10	−58	105	6	DA	7650	13.00	13.32	61.11	34.74	2.7 m
162712.99+002818.6	17.38	0.78	0.31	0.06	−0.01	0.47	−194	−73	6	DA	5983	14.08	14.49	44.31	43.54	2.7 m
162731.09+485919.0	19.19	1.51	0.59	0.24	0.05	0.07	−91	77	6	DZA	5105	14.78	15.43	58.01	32.78	MMT
164847.07+393917.0	18.81	1.29	0.54	0.16	0.06	0.07	−126	0	6	DC	5401	14.53	15.08	56.98	34.03	MMT
165445.70+382936.6	16.93	0.96	0.40	0.15	0.02	0.08	18	−325	5	DZA	5847	14.18	14.62	29.72	45.85	2.7 m
165940.00+320320.1	17.56	0.63	0.28	0.07	0.01	0.16	−238	−244	6	DA	6428	13.76	14.12	51.35	82.96	2.7 m
170447.70+360847.4	18.63	1.79	0.75	0.28	0.12	0.13	186	−175	6	DC	4560	15.28	16.13	33.21	40.20	HET
171433.26+273836.1	18.16	0.40	0.12	0.01	−0.11	0.24	49	−20	6	DC	7235	13.24	13.57	89.96	22.57	2.7 m
172257.78+575250.7	19.17	1.14	0.46	0.23	0.06	0.15	−37	390	6	DC	5403	14.53	15.08	69.64	129.32	HET
172413.32+275655.2	17.47	0.78	0.30	0.11	0.00	0.26	47	−60	6	DA	6131	13.97	14.37	45.61	16.48	2.7 m
172807.29+264620.1	18.02	0.97	0.42	0.16	0.04	0.23	−45	−255	6	DA	5619	14.36	14.85	46.57	57.15	2.7 m
204128.99−052027.7	19.09	1.65	0.70	0.26	0.06	0.26	−149	−29	6	DC	4673	15.17	15.98	45.68	32.87	MMT
204259.23+003156.6	19.67	1.65	0.81	0.30	0.07	0.37	−71	−244	6	DC	4201	15.63	16.57	47.29	56.96	HET
204506.97+003734.4	19.43	0.59	0.25	0.12	0.00	0.45	32	−32	6	DA	6093	14.00	14.40	117.73	25.25	MMT
204557.53−071003.5	19.08	1.61	0.68	0.21	0.12	0.39	−73	−134	6	DC	4682	15.16	15.97	47.90	34.65	MMT
210330.85−002446.4	18.22	0.66	0.27	0.07	0.02	0.34	61	−139	6	DC	6223	13.91	14.29	68.61	49.36	MMT
211640.30−072452.7	17.93	1.67	0.69	0.25	0.05	0.70	111	−223	6	DC	4359	15.47	16.38	25.89	30.56	2.7 m
211805.21−073729.1	19.85	2.42	0.98	0.33	0.11	1.17	115	−144	5	DC	3401	16.55	17.37	43.44	37.95	HET
211858.65+112017.7	18.13	0.77	0.27	0.09	0.01	0.42	359	−13	5	DA	6086	14.00	14.40	64.24	109.38	2.7 m
212501.48−073456.0	19.48	0.74	0.26	0.08	0.01	0.56	64	13	5	DA	6063	14.02	14.42	122.54	37.93	MMT
213643.08−070638.2	19.43	0.60	0.25	0.08	−0.03	0.20	69	−11	5	DA	6520	13.70	14.05	125.93	41.71	MMT

TABLE 1—*Continued*

Object (SDSS J) (1)	g (2)	$u-g$ (3)	$g-r$ (4)	$r-i$ (5)	$i-z$ (6)	A_u (7)	$\mu_{\rm R.A.}$ (8)	$\mu_{\rm decl}$ (9)	Epochs (10)	Type (11)	$T_{\rm eff}$ (12)	$M_{\rm bol}$ (13)	M_g (14)	D (15)	V_T (16)	Source (17)
214752.10−082436.8	17.59	0.75	0.32	0.14	−0.01	0.24	30	153	6	DA	6010	14.06	14.47	45.77	33.82	2.7 m
215430.69+130026.7	18.75	1.55	0.61	0.25	0.10	0.41	367	−73	6	DZA	4768	15.08	15.86	43.76	77.62	MMT
215501.53+120116.4	18.47	0.65	0.25	0.07	−0.06	0.54	−76	−25	4	DA	6121	13.98	14.37	79.14	30.01	MMT
220414.16−010931.2	19.88	1.88	0.83	0.24	0.11	0.44	112	−303	6	DC	4189	15.65	16.58	52.87	80.95	HET
222233.90+122143.0	19.13	1.95	1.02	0.36	0.18	0.41	731	198	4	DC	3448	16.49	17.33	25.78	92.53	HET
224157.63+133238.8	17.36	0.82	0.35	0.10	0.02	0.26	61	−395	6	DA	5986	14.07	14.49	40.90	77.49	2.7 m
224206.19+004822.8	19.38	2.43	0.91	0.34	0.08	0.36	132	−76	6	DC	3407	16.55	17.37	29.12	21.02	HET
225408.64+132357.2	19.33	2.04	0.97	0.33	0.10	0.26	329	−199	6	DC	3356	16.61	17.41	26.72	48.71	HET
231206.08+131057.6	17.45	1.38	0.56	0.16	0.08	0.38	−132	−256	6	DA	5078	14.80	15.46	28.40	38.78	2.7 m
232519.89+140339.7	16.30	1.55	0.57	0.27	0.09	0.23	336	115	6	DC	4941	14.92	15.63	14.80	24.92	2.7 m
233040.47+010047.4	17.36	0.64	0.17	0.06	0.02	0.20	−255	−125	6	DA	6768	13.54	13.88	53.63	72.19	2.7 m
233055.20+002852.3	19.77	1.96	0.89	0.30	0.11	0.17	151	91	6	DC	4126	15.71	16.65	44.42	37.12	HET
233707.68+003242.3	18.13	1.01	0.45	0.14	−0.02	0.18	305	162	6	DA	5629	14.35	14.84	48.35	79.15	2.7 m
234041.47−110636.9.....	18.46	0.53	0.25	0.74	0.85	0.15	19	−87	6	DA + M	6612	13.64	13.99	82.58	34.86	MMT
234245.75−100121.4	18.83	1.52	0.71	0.26	0.04	0.16	−28	−95	6	DA	4719	15.12	15.92	40.18	18.86	MMT
235042.52−084618.9	19.03	1.04	0.50	0.22	0.08	0.18	209	−139	6	DA	5298	14.61	15.20	62.18	73.97	HET
235416.59+003001.2	19.25	0.71	0.20	0.10	0.04	0.20	53	18	5	DA	6568	13.67	14.02	119.10	31.60	MMT

NOTE.—Table 1 is also available in machine-readable form in the electronic edition of the *Astronomical Journal*.

TABLE 2

SPECTROSCOPICALLY IDENTIFIED SUBDWARF STARS

Name (SDSS J)	g	$u-g$	$g-r$	$r-i$	$i-z$	A_u	$\mu_{\rm R.A.}$	$\mu_{\rm decl}$	Epochs	Dist22	Source
001813.74−085458.6	19.48	0.73	0.24	0.07	−0.03	0.23	−41	−33	5	15.1	MMT
002958.84+151841.1	19.20	0.84	0.29	0.08	0.07	0.34	−46	−31	4	30.4	MMT
005331.26+000509.8	19.38	2.18	1.09	0.53	0.23	0.13	137	−22	6	24.4	MMT
010502.05+140154.4	19.40	1.00	0.43	0.15	0.08	0.37	−11	48	5	25.4	MMT
013119.61+000257.6	17.93	2.18	1.14	0.45	0.25	0.17	230	−115	6	31.0	2.7 m
014833.19−011043.3	17.98	1.91	0.85	0.36	0.15	0.17	152	−106	6	13.8	2.7 m
015632.67+144729.7	17.48	1.52	0.66	0.27	0.07	0.29	111	−95	5	7.8	2.7 m
021213.80+000042.1	18.81	1.33	0.51	0.21	0.10	0.16	81	61	5	12.9	MMT
022947.61−085020.2	16.80	1.62	0.74	0.24	0.14	0.17	151	−95	6	6.4	2.7 m
023807.99−093033.6	18.61	1.87	0.77	0.30	0.19	0.15	80	−46	6	29.4	MMT
030048.83−004408.0	17.21	1.20	0.60	0.26	0.19	0.60	83	−113	6	12.6	2.7 m
030722.43+003405.2	15.68	1.18	0.49	0.18	0.08	0.55	156	−109	6	41.2	2.7 m
031043.74−081848.7	17.49	0.86	0.25	0.08	0.03	0.36	−32	48	5	13.4	2.7 m
031845.08−061236.3	16.56	1.51	0.73	0.28	0.18	0.33	159	−104	6	35.0	2.7 m
035147.74−053302.9	15.94	1.54	0.74	0.28	0.12	0.56	237	−264	6	31.9	2.7 m
073636.05+290222.7	17.41	1.11	0.34	0.13	0.05	0.24	−18	−71	5	4.6	2.7 m
073856.39+322518.9	17.52	1.73	0.80	0.33	0.16	0.22	5	−144	6	17.0	2.7 m
075217.25+252155.6	16.79	1.03	0.27	0.07	0.00	0.40	146	214	4	26.2	2.7 m
080005.13+460801.1	16.64	1.13	0.55	0.16	0.11	0.38	−2	309	4	19.6	2.7 m
081306.76+023425.9	17.15	1.30	0.45	0.19	0.09	0.14	309	−45	5	7.7	2.7 m
083049.85+025018.6	18.24	1.55	0.53	0.12	0.12	0.17	45	87	6	5.5	2.7 m
083743.43+020101.7	17.91	2.14	0.78	0.30	0.11	0.25	−15	−443	4	5.5	MMT
090513.97+473728.5	18.67	2.79	1.33	0.51	0.31	0.08	−159	−344	6	35.1	MMT
091909.52+564100.1	17.03	2.09	0.70	0.24	0.14	0.17	1	−263	5	10.0	2.7 m
093559.33+601323.0	17.22	1.40	0.55	0.25	0.09	0.15	−4	−275	4	11.3	2.7 m
095926.92−000849.7	16.82	2.03	0.79	0.31	0.09	0.16	−315	90	5	6.0	2.7 m
100537.72+525913.2	17.30	0.95	0.24	0.08	−0.01	0.04	−3	131	5	12.1	2.7 m
100633.59−002732.4	17.95	1.01	0.47	0.16	0.08	0.19	−237	−72	5	4.1	2.7 m
101739.82+020933.8	16.79	1.40	0.59	0.21	0.12	0.25	−240	190	4	16.5	2.7 m
104149.72+624455.6	16.69	0.98	0.29	0.08	0.05	0.03	55	161	5	12.2	2.7 m
105157.48+020300.4	19.74	1.97	1.05	0.46	0.28	0.22	166	−105	5	32.0	MMT
110723.94+622606.0	16.29	0.97	0.33	0.11	0.03	0.05	46	239	4	25.4	2.7 m
111327.37+585848.5	17.09	2.32	1.24	0.48	0.31	0.05	−296	−472	6	59.0	2.7 m
112204.68+655359.7	17.54	1.08	0.36	0.17	0.04	0.06	−63	−152	5	39.5	2.7 m
113102.89+665751.2	16.66	1.64	0.52	0.25	0.11	0.05	−116	206	5	42.9	2.7 m
113512.08+032841.2	19.24	2.80	1.18	0.47	0.31	0.11	−163	−255	6	20.1	MMT
115206.86+670204.2	16.33	0.87	0.21	0.08	0.02	0.06	−117	143	4	19.8	2.7 m
120945.96+630243.9	16.96	0.86	0.25	0.08	0.01	0.10	−71	196	5	26.5	2.7 m
125047.35+032652.8	18.28	2.17	0.98	0.43	0.19	0.16	−97	−221	4	12.5	2.7 m
125226.29+022838.8	16.78	1.44	0.49	0.16	0.05	0.16	155	−100	5	19.1	2.7 m
130507.26+041408.1	16.81	0.92	0.32	0.12	0.02	0.13	−135	−47	5	9.3	2.7 m
134233.44+580019.7	17.16	1.08	0.32	0.13	0.04	0.04	15	196	5	15.7	2.7 m
140635.95+615335.6	19.70	1.96	1.03	0.42	0.25	0.07	−84	296	5	36.2	HET
163716.86+451701.8	17.79	0.95	0.33	0.08	0.05	0.06	−83	−414	4	13.6	2.7 m
170206.35+314749.9	17.71	1.57	0.58	0.19	0.13	0.21	246	−99	5	9.6	2.7 m
171737.03+623448.1	18.26	1.10	0.32	0.16	0.00	0.12	−36	43	6	28.5	2.7 m
171918.54+291538.6	17.52	1.55	0.59	0.14	0.08	0.20	72	142	5	11.1	2.7 m
173552.77+573814.3	17.88	2.07	1.00	0.40	0.19	0.33	−89	156	6	20.0	2.7 m
205859.24−055703.8	19.16	1.51	0.59	0.19	0.08	0.23	−51	51	4	12.1	MMT
213427.61−081511.0	18.41	1.34	0.49	0.15	0.08	0.18	−75	19	5	23.0	MMT
214239.11−005550.3	18.69	2.41	1.19	0.47	0.26	0.27	103	−173	6	13.6	MMT
214819.02+003943.2	18.30	0.99	0.35	0.10	0.01	0.81	−55	79	6	9.7	MMT
221428.87+135341.9	17.66	1.04	0.39	0.14	0.06	0.33	90	50	6	8.7	2.7 m
225449.68+125922.6	19.23	1.75	1.00	0.31	0.21	0.20	226	−125	5	7.2	HET
225803.60−100702.0	19.33	2.73	1.08	0.57	0.29	0.20	108	−145	6	28.8	MMT

NOTE.—Proper motions for stars that have not been detected in one or two USNO-B epochs (Ep < 6) or that have a neighbor brighter than 22 mag within 7″ (Dist22 < 7) are unreliable.

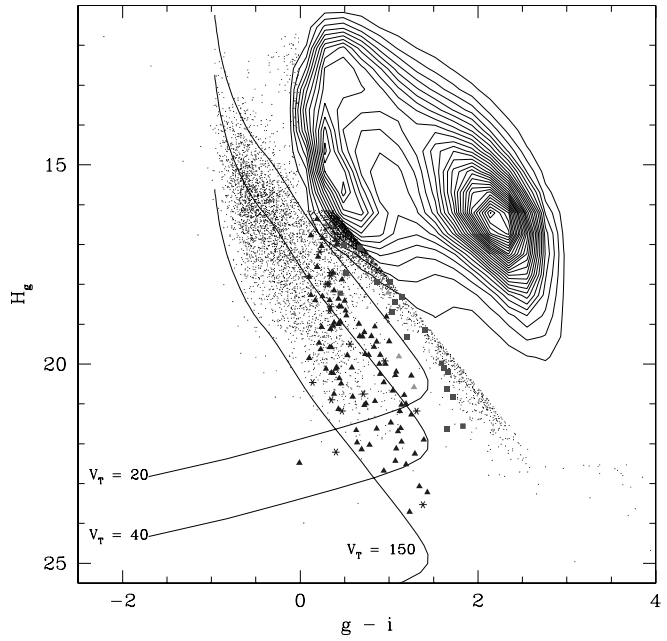

FIG. 6.—Same as Fig. 1, but for the spectroscopically confirmed white dwarfs, white dwarf + late-type star binaries, subdwarfs, and quasars found in our study. White dwarfs that did not meet our criteria for reliable proper motions are plotted as asterisks. [*See the electronic edition of the Journal for a color version of this figure.*]

opacities is incomplete. All being massive is statistically unlikely, as the average mass for cool white dwarfs ($T_{\rm eff} \leq 5000$ K) with trigonometric parallax measurements is $0.61 \pm 0.2\ M_\odot$ (Bergeron et al. 2001). Mixed-atmosphere white dwarfs are expected to show stronger flux deficits in the infrared than pure H white dwarfs (Bergeron et al. 1995); the effects of CIA become significant at warmer temperatures, which could explain the observed blue turnoff of cool white dwarfs in Figure 8 (*bottom*). Bergeron & Leggett (2002) argued that all white dwarfs cooler than 4000 K have mixed H/He atmospheres. In addition, Kilic et al. (2004) suggested that all white dwarfs cooler than 5000 K may have mixed atmospheres. Therefore, this figure presents further evidence that the coolest white dwarfs indeed have helium-rich atmospheres.

4.3. *Non-DA Gap*

The Hα and Hβ equivalent widths of all DA and DC white dwarfs in our sample are shown against $g - r$ in Figure 9. White dwarf models predict that Hα will disappear around $V - I \sim 1.1$ (see Fig. 7 of Bergeron et al. 1997). Although there is a large scatter in our equivalent width measurements in Figure 9, it is apparent that the Hα and Hβ equivalent widths decrease with increasing $g - r$ color, and they vanish around $g - r \sim 0.7$ (or $V - I \sim 1.1$), in good agreement with the model predictions. The scatter in the equivalent width measurements may be partly due to variations in gravities and the use of spectra with different signal-to-noise ratios from four different telescope + instrument combinations.

Bergeron et al. (1997, 2001) argued that most of the white dwarfs with $T_{\rm eff}$ in the range 5000–6000 K are of DA type, and they found evidence for a so-called non-DA gap. Even though non-DA stars are seen above and below this temperature range,

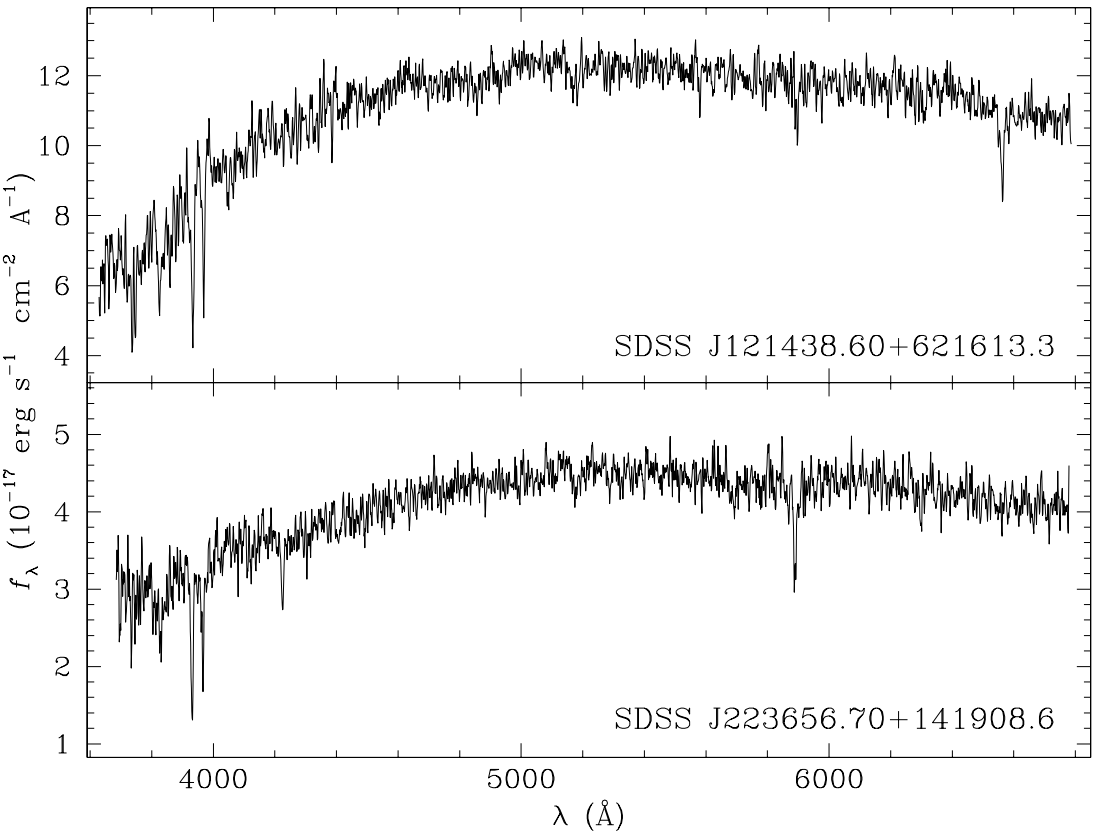

FIG. 7.—MMT spectra for two uncertain white dwarfs/subdwarfs.

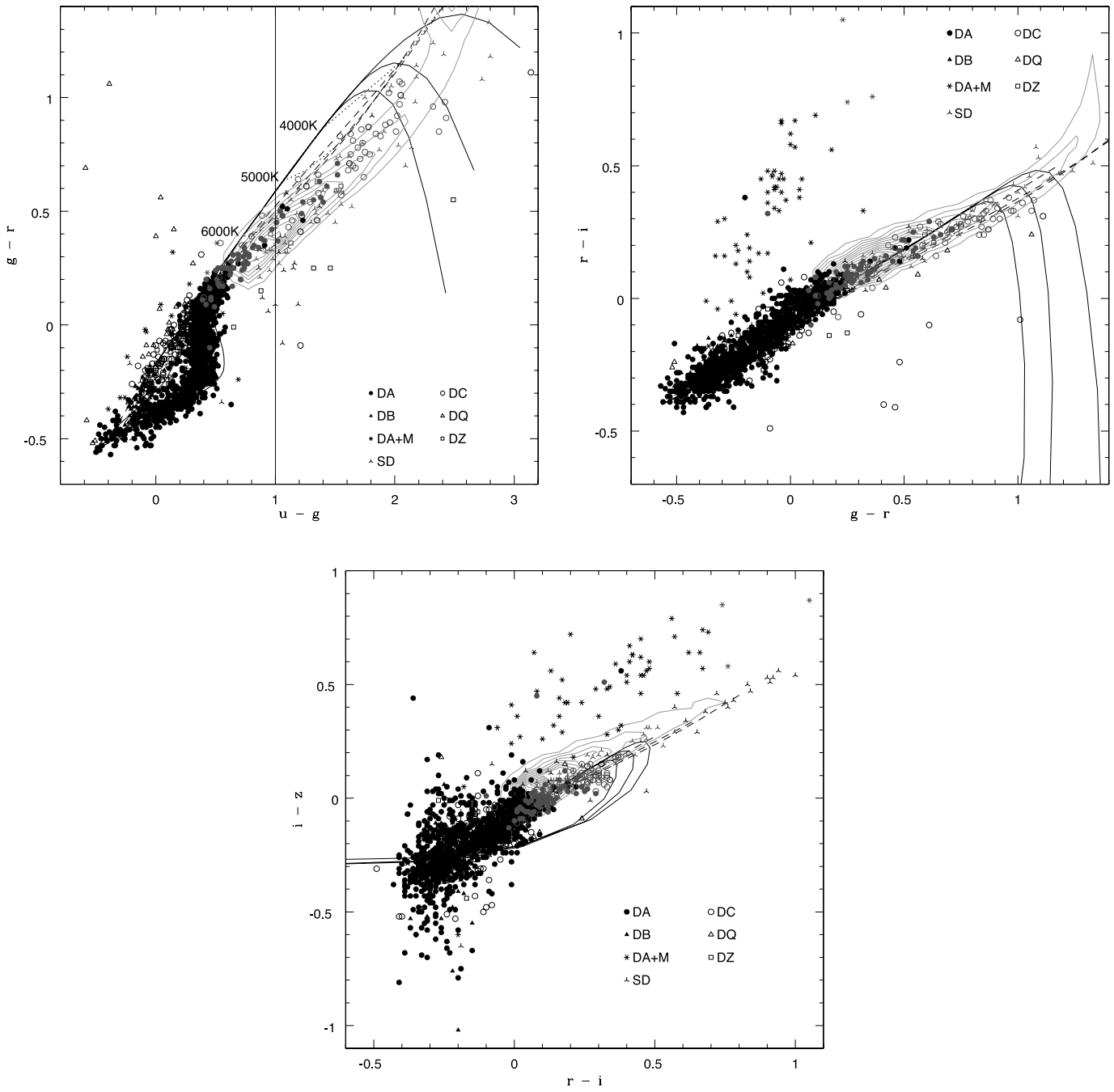

FIG. 8.—Color-color diagrams showing the white dwarfs and subdwarfs from our study (*light symbols*) and the literature (*black symbols*). Different types of white dwarfs are shown with different symbols. The contours represent objects without spectroscopic confirmation. The curves show the colors of white dwarf model atmospheres (P. Bergeron 2001, private communication) of pure H (*solid curves*) and pure He (*dashed curves*) with $\log g = 7$, 8, and 9, where the $\log g = 9$ curve is the bottom and $\log g = 7$ is the top curve in the top left panel. The dotted lines with labels connect models with the same effective temperature. [*See the electronic edition of the Journal for a color version of this figure.*]

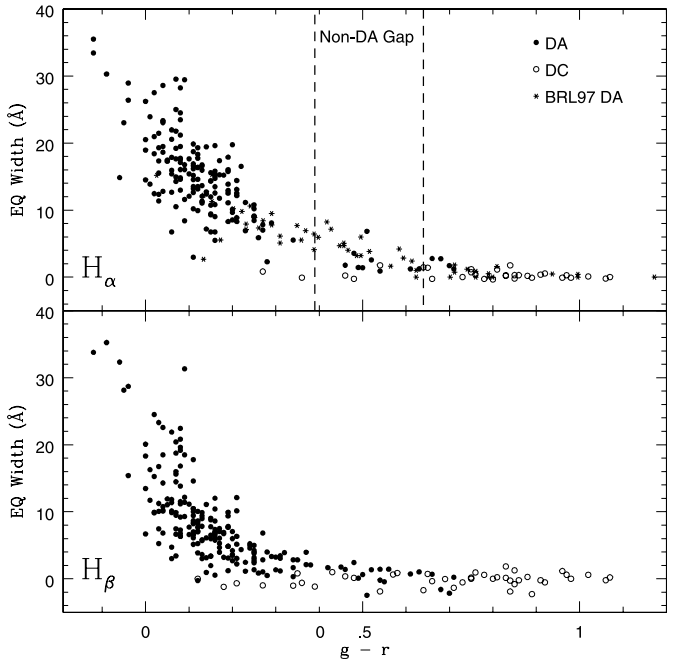

FIG. 9.—Equivalent width measurements of Hα and Hβ as a function of $g - r$ for the DA and DC white dwarfs in our sample. The top panel also includes Hα equivalent width measurements of the Bergeron et al. (1997) DA sample. The predicted non-DA gap for $\log g = 8$ DA white dwarfs is marked by the dashed lines. Since McDonald 2.7 m telescope spectra do not cover Hα, we do not have Hα equivalent width measurements for some of our objects.

they found only two peculiar non-DA stars inside the gap. Bergeron et al. (1997, 2001) and Hansen (1999) tried to explain the existence of this gap in terms of different physical mechanisms, i.e., convective mixing and different evolutionary timescales of hydrogen-rich and helium-rich white dwarfs. The existence of the non-DA gap is apparent in Bergeron et al.'s (2001) $V - I$ versus $V - K$ color-color diagram. Figure 10 shows $u - g$ versus $g - r$ (*left panels*), $g - r$ versus $r - i$ (*middle panels*), and $r - i$ versus $i - z$ (*right panels*) color-color diagrams for white dwarfs in our sample. The data set is divided into DA (*top panels*) and non-DA (*bottom panels*; DC and DQ) stars. The pure H (DA panels) and pure He (non-DA panels) model sequences with 6000 K $\gtrsim T_{\rm eff} \gtrsim$ 5000 K are also shown for $\log g = 7$ (*solid line*), 8 (*dashed line*), and 9 (*dotted line*). The two differences between these color-color diagrams and Figure 8 are that (1) DC white dwarfs discovered at the McDonald 2.7 m telescope are not included in Figure 10, since the 2.7 m telescope spectra do not cover Hα, and so some of the white dwarfs observed with the 2.7 m telescope and classified as DCs may turn out to be DAs showing Hα only, and (2) ultracool white dwarfs discovered in the SDSS are not included. SDSS J1001+3903, an ultracool white dwarf discovered by Gates et al. (2004), falls in the non-DA gap in the $u - g$ versus $g - r$ diagram but not in the other two diagrams. Even though ultracool white dwarfs are predicted to have $T_{\rm eff} \leq 4000$ K, they mimic bluer/warmer objects in the various color-color diagrams and therefore are not included in this discussion.

DA white dwarfs show Hα absorption for $g - r \leq 0.7$ ($\geq$5000 K), and we should have detected Hα for DCs with 6000 K $\gtrsim T_{\rm eff} \gtrsim$ 5000 K if they had pure H atmospheres. The Hα panel in Figure 9 shows exactly three DC stars in the gap. (The gap, marked by the dashed lines, is $g - r = 0.39$–0.64 for hydrogen atmospheres.) Based on *ugriz* photometry (Fig. 10), we see DC stars above and below the non-DA gap, but we find only three to five DC stars (*bottom panels, filled circles*) in the gap. All these white dwarfs (SDSS J0157+1335, J1203+0426, J1205+0449, J1648+3939, and J1722+5752) are observed at the MMT and HET, and Balmer lines cannot be seen in their spectra. Assuming pure He composition, we estimate their temperatures to be 5254, 5144, 5635, 5536, and 5555 K (see § 4.4 for temperature estimates). These stars appear to be non-DA stars in the 5000–6000 K temperature range and fill in the Bergeron et al. (1997, 2001) non-DA gap to some extent. The fraction of DA/non-DA stars in this temperature range is still seen to be large in our data, and further data are needed to quantify the ratio. Moreover, Bergeron et al. (1997) have identified a group of DC white dwarfs that lie close to $T_{\rm eff} = 6000$ K whose energy distributions are better reproduced with pure H models. Therefore, some or all of these stars may be explained with hydrogen-rich compositions. Bergeron et al. (2001) and Ruiz & Bergeron (2001) showed that infrared photometry is needed to discriminate between hydrogen-rich and helium-rich atmospheres for cool white dwarfs; infrared photometry is needed to reliably determine the spectral types and temperatures for these stars. In any case, our data support at least a deficit in the number of non-DA white dwarfs in the predicted non-DA gap.

4.4. *Model Atmosphere Analysis*

The u, g, r, i, and z photometry for each of the new spectroscopically confirmed white dwarfs has been fitted with synthetic photometry predicted from the model atmospheres (P. Bergeron 2001, private communication), using a minimum χ^2 fit. Since trigonometric parallax measurements are not available for these white dwarfs, a value of $\log g = 8.0$ has been assumed for all objects. Due to larger uncertainties in u and z, and the fact that the u magnitudes of cool white dwarfs are affected by an unexplained UV opacity source, u and z magnitudes are given lower weight in our fits. The fits have been done using only u, g, and r magnitudes for white dwarf + late-type star binaries, although some of these binaries may have contaminated u, g, and r magnitudes.

While spectra of bluer white dwarfs allow us to determine whether the atmosphere is hydrogen-rich or helium-rich, Hα and Hβ disappear around $g - r \sim 0.7$, and so IR photometry is needed to determine the atmospheric composition for DCs. We assume hydrogen-rich composition for the analysis of all the DA and DC white dwarfs in our sample. Figure 11 shows the effects of using hydrogen-rich versus helium-rich composition models on our temperature estimates for the DC stars in our sample. Both hydrogen-rich and helium-rich models give similar answers for stars with $T_{\rm eff}$ in the range 10,000–5500 K ($g - i < 0.7$), although the effect drastically increases below 5500 K due to the onset of CIA. Pure He models predict warmer temperatures than the pure H models; the optical colors of a 4000 K pure H atmosphere white dwarf can be fitted with a 4700 K pure He white dwarf model.

We assumed zero reddening for white dwarfs with estimated distances $\leq$100 pc and used the full reddening value from Schlegel et al. (1998) if the estimated distance from the Galactic plane was larger than 250 pc. For white dwarfs with estimated distances between 100 and 250 pc, we used a linear interpolation between zero and the full reddening coefficient.

Results of the model atmosphere fits are summarized in columns (12)–(16) of Table 1. For each white dwarf, we give (assuming pure H composition with $\log g = 8.0$) the effective temperature, the predicted bolometric magnitude, the absolute magnitude in g, the distance, and the estimated tangential velocity. According to our fits, there are seven white dwarfs with $T_{\rm eff} \leq 4000$ K in our sample, but these temperature estimates are questionable, and IR photometry is needed to obtain reliable results for these objects. Although most of the newly found

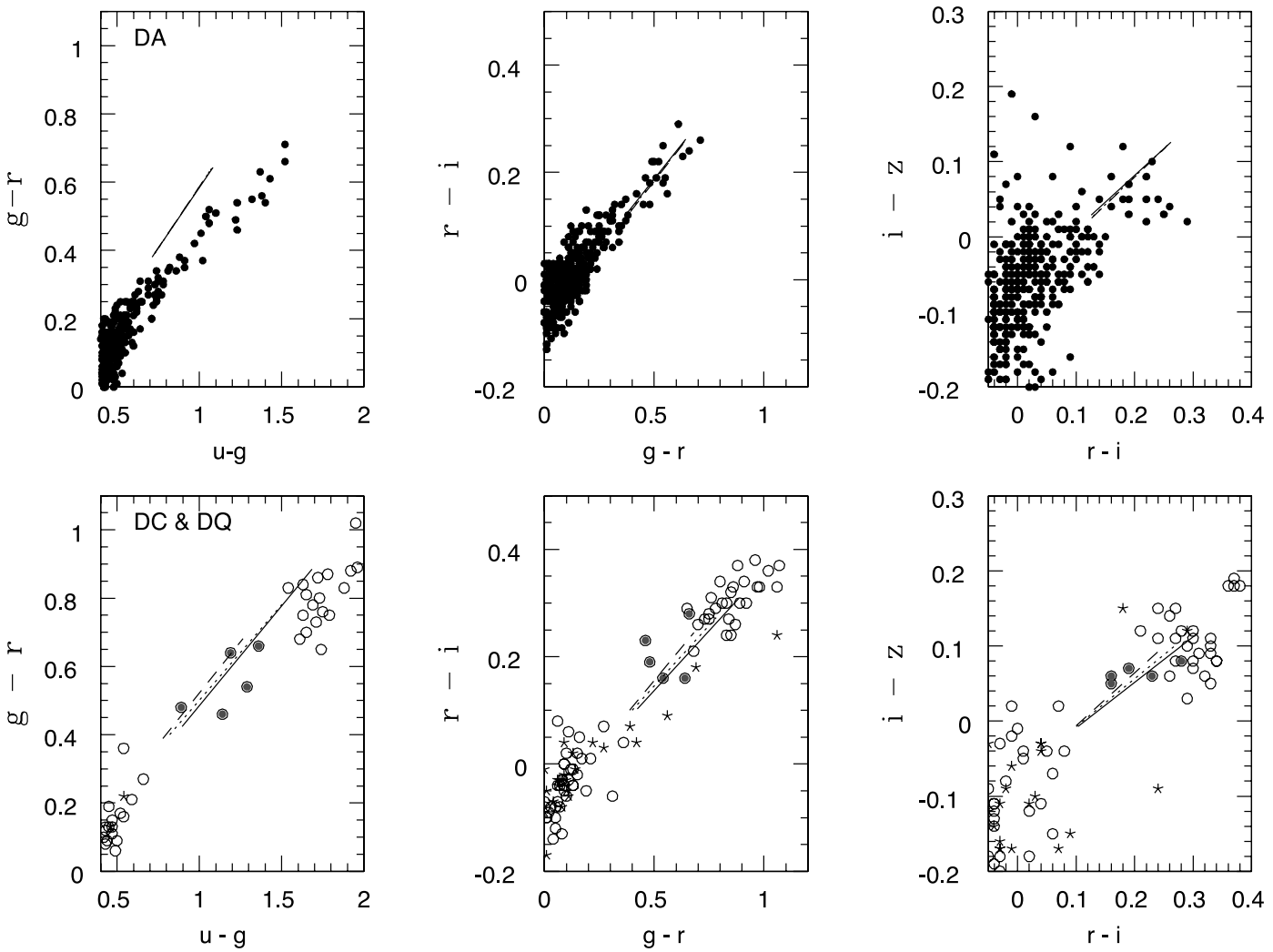

FIG. 10.—The $u - g$ vs. $g - r$ (*left panels*), $g - r$ vs. $r - i$ (*middle panels*), and $r - i$ vs. $i - z$ (*right panels*) color-color diagrams for white dwarfs in our sample. The top panels show DA white dwarfs, whereas the bottom panels show DC (*open circles*) and DQ (*stars*) white dwarfs. The pure H (DA panels) and pure He (non-DA panels) model sequences with 6000 K $\gtrsim T_{\rm eff} \gtrsim$ 5000 K are also shown for $\log g = 7$ (*solid line*), 8 (*dashed line*), and 9 (*dotted line*). Probable DC white dwarfs in the non-DA gap are shown as filled circles. [*See the electronic edition of the Journal for a color version of this figure.*]

white dwarfs show disk kinematics, there are 16 objects with $V_T \geq 150$ km s^{-1} that may be halo white dwarfs. Halo membership of these objects and several others from the SDSS Data Release 3 are discussed in Harris et al. (2006).

5. CONCLUSIONS AND FUTURE WORK

SDSS photometry and SDSS + USNO-B astrometry (Munn et al. 2004) have been used to isolate cool white dwarf candidates in a reduced proper motion diagram in the SDSS DR2. Using SDSS spectra and follow-up spectroscopy on the MMT, HET, and McDonald 2.7 m telescope, we showed that the white dwarf locus in the reduced proper motion diagram is cleanly separated from the far more numerous subdwarfs, with a contamination rate due to falsely measured large proper motions of only 1%–2%. In a companion paper, Harris et al. (2006) use this clean separation of white dwarfs in the reduced proper motion diagram to assemble a statistically complete sample of white dwarfs in the SDSS Data Release 3 and determine the white dwarf luminosity function. The detailed shape of this new luminosity function will eventually make it possible to study the cooling physics of white dwarfs in detail, e.g., neutrino cooling, crystallization, and phase separation. These effects produce overlapping signatures (bumps) in the white dwarf luminosity function that can be used to calibrate their significance. The details of this constituent input physics can affect the implied ages of cool white dwarfs below $\log (L/L_{\odot}) \sim -4.2$ by as much as 2–3 Gyr (Knox et al. 1999; Montgomery et al. 1999; Salaris et al. 2000).

All the ultracool white dwarfs discovered in SDSS (Harris et al. 2001; Gates et al. 2004) show significant proper motion; hence, they would be discovered in our proper-motion survey if not targeted by SDSS fiber spectroscopy. We have discovered seven new cool white dwarfs with estimated temperatures below 4000 K. Nevertheless, these objects may have temperatures above 4000 K if they have pure He atmospheres (see Fig. 11). Our spectroscopy from the HET and the MMT does not go red enough to detect the CIA in the near-IR, although all these objects and several others should show infrared flux deficiency due to CIA if they have pure H or mixed H/He atmospheres. Our SDSS DR2 proper-motion catalog does not reveal any other ultracool white dwarf candidate exhibiting strong CIA absorption. Therefore, SDSS J1337+00, LHS 3250, and SDSS J0947+44 are the only ultracool white dwarfs (within our magnitude limit) showing strong CIA absorption in the SDSS DR2 imaging area (3324 deg^2). Further progress in understanding the ultracool white dwarfs and estimating reliable temperatures for our cool white dwarf sample can be achieved with the help of *JHK* infrared

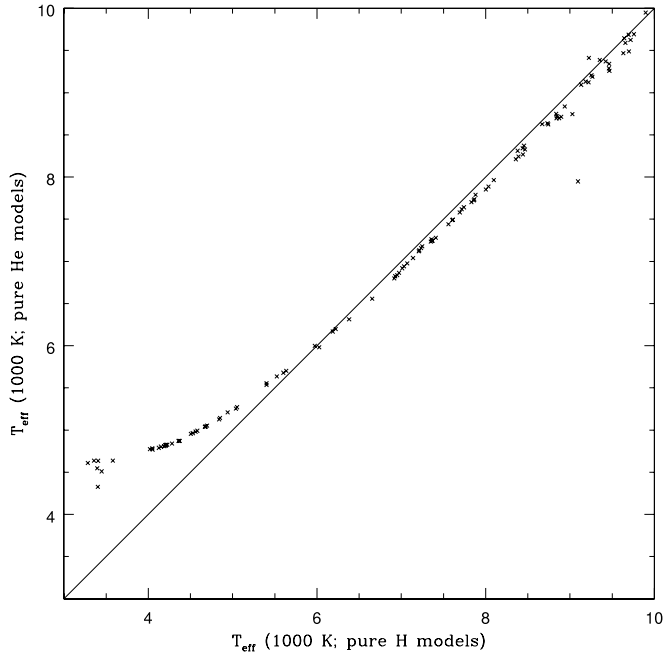

FIG. 11.—Effective temperatures for our sample of DC white dwarfs using pure H or pure He white dwarf model atmospheres. The effects of using a hydrogen-rich or a helium-rich composition to estimate temperatures become significant below ~5500 K.

photometric observations. We have begun such a program at the NASA Infrared Telescope Facility. Trigonometric parallax measurements for these white dwarfs will also be necessary to measure their masses.

Even though our survey has a fainter magnitude limit and a lower proper motion cutoff than the Luyten half-second survey, the faint end of the white dwarf luminosity function at which most of the age sensitivity resides is still poorly populated. The magnitude limit of the SDSS + USNO-B proper-motion catalog is set by the photographic POSS I and POSS II plates. Although SDSS imaging is 95% complete down to $g = 22$, the SDSS + USNO-B proper-motion catalog is only 90% complete down to $g = 19.7$. A second-epoch CCD imaging survey in r or i to 22 mag may be necessary to find the coolest white dwarfs in the disk and possible halo white dwarfs (von Hippel et al. 2005). Also, we may be missing slowly moving cool white dwarfs; a kinematically unbiased control sample, e.g., DDO51 photometry + multiobject spectroscopy (Kilic et al. 2004), would be useful to check the completeness of our survey.

This material is based on work supported by the National Science Foundation under grants AST 03-07315 (to T. v. H., D. E. W., and M. K.) and AST 03-07321 (to J. L. and K. A. W.). We thank Pierre Bergeron and Didier Saumon for making their model atmospheres available to us. We also thank Harry Shipman for careful reading of this manuscript. The Hobby-Eberly Telescope (HET) is a joint project of the University of Texas at Austin, Pennsylvania State University, Stanford University, Ludwig-Maximilians-Universität München, and Georg-August-Universität Göttingen. The HET is named in honor of its principal benefactors, William P. Hobby and Robert E. Eberly. The Marcario Low Resolution Spectrograph (LRS) is named for Mike Marcario of High Lonesome Optics, who fabricated several optics for the instrument but died before its completion. The LRS is a joint project of the HET partnership and the Instituto de Astronomía de la Universidad Nacional Autonoma de México.

Funding for the Sloan Digital Sky Survey (SDSS) has been provided by the Alfred P. Sloan Foundation, the Participating Institutions, the National Aeronautics and Space Administration, the National Science Foundation, the US Department of Energy, the Japanese Monbukagakusho, and the Max Planck Society. The SDSS Web site is at http://www.sdss.org.

The SDSS is managed by the Astrophysical Research Consortium for the Participating Institutions. The Participating Institutions are the University of Chicago, Fermilab, the Institute for Advanced Study, the Japan Participation Group, the Johns Hopkins University, the Korean Scientist Group, Los Alamos National Laboratory, the Max Planck Institute for Astronomy, the Max Planck Institute for Astrophysics, New Mexico State University, the University of Pittsburgh, Princeton University, the United States Naval Observatory, and the University of Washington.

REFERENCES

Abazajian, K., et al. 2003, AJ, 126, 2081
———. 2004, AJ, 128, 502
Bergeron, P. 2003, ApJ, 586, 201
Bergeron, P., & Leggett, S. K. 2002, ApJ, 580, 1070
Bergeron, P., Leggett, S. K., & Ruiz, M. T. 2001, ApJS, 133, 413
Bergeron, P., Ruiz, M. T., & Leggett, S. K. 1997, ApJS, 108, 339
Bergeron, P., Saumon, D., & Wesemael, F. 1995, ApJ, 443, 764
Claver, C. F. 1995, Ph.D. thesis, Univ. Texas
Dahn, C. C., Monet, D. G., & Harris, H. C. 1989, in IAU Colloq. 114, White Dwarfs, ed. G. Wegner (Berlin: Springer), 24
Fan, X. 1999, AJ, 117, 2528
Fleming, T. A., Liebert, J., & Green, R. F. 1986, ApJ, 308, 176
Gates, E., et al. 2004, ApJ, 612, L129
Hansen, B. M. S. 1998, Nature, 394, 860
———. 1999, ApJ, 520, 680
Harris, H. C., et al. 2001, ApJ, 549, L109
———. 2003, AJ, 126, 1023
———. 2006, AJ, 131, 571
Hogg, D. W., Finkbeiner, D. P., Schlegel, D. J., & Gunn, J. E. 2001, AJ, 122, 2129
Kilic, M., Winget, D. E., von Hippel, T., & Claver, C. F. 2004, AJ, 128, 1825
Kleinman, S. J., et al. 2004, ApJ, 607, 426
Knox, R. A., Hawkins, M. R. S., & Hambly, N. C. 1999, MNRAS, 306, 736
Lépine, S., Shara, M. M., & Rich, R. M. 2003, AJ, 126, 921
Liebert, J. 1979, in IAU Colloq. 53, White Dwarfs and Variable Degenerate Stars, ed. H. M. van Horn & V. Weidemann (Rochester: Univ. Rochester), 146
Liebert, J., Bergeron, P., & Holberg, J. 2005, ApJS, 156, 47
Liebert, J., Dahn, C. C., & Monet, D. G. 1988, ApJ, 332, 891
Luyten, W. J. 1918, Lick Obs. Bull., 10, 135
———. 1979a, A Catalogue of Stars with Proper Motions Exceeding 0″.5 Annually (Minneapolis: Univ. Minnesota Press)
———. 1979b, New Luyten Two Tenths Catalog (Minneapolis: Univ. Minnesota Press) (NLTT)
Monet, D. G., et al. 2003, AJ, 125, 984
Montgomery, M. H., Klumpe, E. W., Winget, D. E., & Wood, M. A. 1999, ApJ, 525, 482
Munn, J. A., et al. 2004, AJ, 127, 3034
Oppenheimer, B. R., Hambly, N. C., Digby, A. P., Hodgkin, S. T., & Saumon, D. 2001, Science, 292, 698
Oswalt, T. D., Smith, J. A., Wood, M. A., & Hintzen, P. 1996, Nature, 382, 692
Pier, J. R., et al. 2003, AJ, 125, 1559
Reid, I. N., Sahu, K. C., & Hawley, S. L. 2001, ApJ, 559, 942
Reylé, C., Robin, A. C., & Crézé, M. 2001, A&A, 378, L53
Ruiz, M. T., & Bergeron, P. 2001, ApJ, 558, 761
Salaris, M., García-Berro, E., Hernanz, M., Isern, J., & Saumon, D. 2000, ApJ, 544, 1036
Saumon, D., & Jacobson, S. B. 1999, ApJ, 511, L107
Schlegel, D. J., Finkbeiner, D. P., & Davis, M. 1998, ApJ, 500, 525

Schneider, D. P., et al. 2003, AJ, 126, 2579
Silvestri, N. M., Oswalt, T. D., & Hawley, S. L. 2002, AJ, 124, 1118
Smith, J. A., et al. 2002, AJ, 123, 2121
Spagna, A., Carollo, D., Lattanzi, M. G., & Bucciarelli, B. 2004, A&A, 428, 451
von Hippel, T., et al. 2005, in ASP Conf. Ser. 334, 14th European Workshop on White Dwarfs, ed. D. Koester & S. Moehler (San Francisco: ASP), 3
Winget, D. E., Hansen, C. J., Liebert, J., Van Horn, H. M., Fontaine, G., Nather, R. E., Kepler, S. O., & Lamb, D. Q. 1987, ApJ, 315, L77
Wolff, B., Koester, D., & Liebert, J. 2002, A&A, 385, 995
York, D. G., et al. 2000, AJ, 120, 1579